# TECHNICAL REPORT No. 44

# NUMERICAL EXPERIMENTS ON THE SIMULATION OF THE 1979 ASIAN SUMMER MONSOON

by

U.C. Mohanty[1], R.P. Pearce[2] and M. Tiedtke

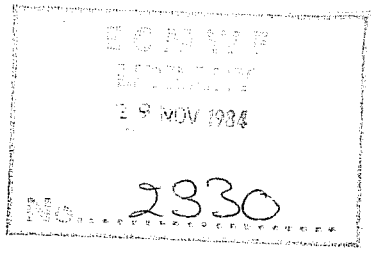


October 1984

[1] Visiting Scientist from
Centre for Atmospheric Sciences
Indian Institute of Technology
Delhi, India.

[2] Department of Meteorology
Reading University
Reading, U.K.

## Abstract

This paper describes the results of three experimental integrations of the ECMWF operational prediction model carried out to examine its ability to predict the onset and subsequent development of the 1979 Asian summer monsoon. Each integration started from 12Z on 11 June, the date of onset of monsoon rains over South India. The first extended over 50 days and included a monsoon 'break'. The other two integrations, each of ten days, were carried out to compare the simulation of the onset by the model using different convection schemes, proposed by Kuo and Arakawa-Schubert (A-S).

Moisture, enthalpy and wind analyses of the predictions are compared with FGGE analyses, with particular emphasis on the Arabian sea region. These show that the rapid intensification of the low level wind there, associated with the monsoon onset, was not reproduced in any of the predictions although the A-S scheme was somewhat more successful. Both schemes tended to establish the main regions of convection too far to the East, off Sri Lanka. The main sources of error are discussed, including initialisation procedures. It is concluded that the main source of error in simulating the summer monsoon onset is the failure of the convection schemes to provide latent heat release in the correct locations.

C O N T E N T S

## 1. INTRODUCTION

This report extends the analysis described by Simmons (1982) of a series of 10-day forecasts and a longer period integration using the ECMWF prediction model. Advantage has been taken of the availability of software developed for a diagnostic study of the Asian summer monsoon onsets during 1979 (using FGGE data) and subsequent years (using ECMWF archived operational analyses), described by Pearce and Mohanty (1984). This has enabled analyses to be carried out of the simulated moisture and enthalpy budgets, as well as of flow fields, and to compare these in detail with the FGGE analysed fields. It is these analyses which are described here.

Following a short description of the ECMWF model in Sect. 2, Sect. 3 of this report describes an analysis of a 50-day simulation starting from 12Z 11 June 1979. Penetrative cumulus convection plays an important role in the generation and maintenance of the monsoon. In Sect. 4 we study its role in a numerical simulation experiment. As the convection scale is much smaller than the model resolution, cumulus convection cannot be considered explicitly; all that can be done is to incorporate the statistical effect of populations of cumulus elements on the large-scale flow by means of some form of parameterisation. Several parameterisation schemes have been proposed in the last two decades which differ considerably in their basic design. Though there have been many comparisons of these schemes it is still not possible to be confident about which one is the most realistic and accurate. Therefore it was decided to perform two experiments with two convectional schemes to parameterise penetrative cumulus convection. The schemes chosen were those developed by Kuo (1974) and Arakawa and Schubert (1974).

The report ends with a summary of results and discussion in Sect.5.

## 2. DESCRIPTION OF EXPERIMENTS

### 2.1 Model description

The integrations were performed with the operational ECMWF grid point model, as described by Burridge and Haseler (1977) and by Tiedtke et al. (1979). Its basic features are summarized below.

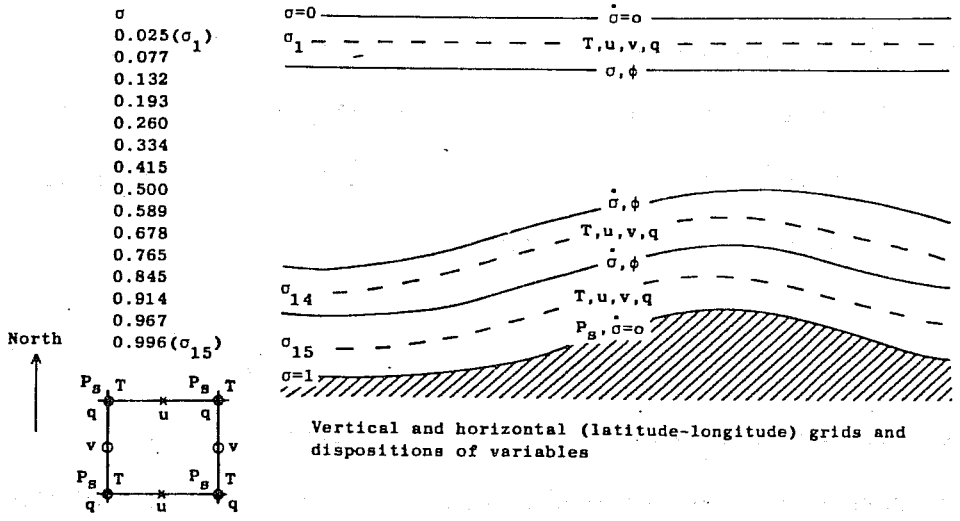


Vertical and horizontal (latitude-longitude) grids and dispositions of variables

| | |
|---|---|
| Independent variables: | $\psi$, $\lambda$, $\sigma$, $t$ |
| Prognostic variables: | $p_s$, T, u, v, q |
| Diagnostic variables: | $\phi$ , $\dot{\sigma} = \frac{d\sigma}{dt}$ |
| Grid: | Arakawa C-grid, N48, uniform in $\lambda$, $\phi$ ($\Delta\lambda = \Delta\phi = 1.875^{o}$)<br>15 levels, non-uniform vertical spacing (see above). |
| Finite difference scheme: | Second order accuracy. |
| Time integration: | Leapfrog, semi-implicit ($\Delta t$ = 15)<br>Weak time filter ($\nu$ = 0.05) |
| Turbulent processes: | Stability dependent vertical diffusion of T, u, v, q, within the surface layer after Monin-Obukov. |
| Cumulus convection: | Kuo (1974) or Arakawa-Schubert (1974). |
| Radiation: | 1. Use of model generated clouds.<br>2. No daily variation of solar radiation. |
| Horizontal diffusion: | Linear 4th order |
| Land surface pressures: | Prognoses of soil temperature, soil water and snow amount. |
| Sea surface temperatures: | Climatologically prescribed. |
| Topography: | Based on US Navy 10' orography adapted to a N48 lat-long grid. |

Experiments were carried out with the cumulus convection parameterised by means of the Kuo-scheme (Kuo, 1974) and the Arakawa-Schubert scheme (Arakawa and Schubert, 1974).

The basic assumption in Kuo's scheme (Kuo, 1965, 1974) is that cumulus convection occurs in layers of conditionally unstable stratification and is maintained by the moisture supply due to large-scale convergence and evaporation from the surface. The environment is convectively heated and moistened by lateral mixing of cloud and environmental air, the amount depending on the local temperature and moisture excess of the cloud ascent over the environment. The net column heating and moistening is assumed to be in equilibrium with the net moisture supply by large-scale convergence and surface evaporation. The Kuo-scheme used in this study is identical to that used in the ECMWF operational forecast model (Tiedtke et al. 1979).

The scheme proposed by Arakawa and Schubert (1974) (referred to as A-S from now on) is one of the most comprehensive cumulus parameterisation schemes. It is based on a theory which describes the interaction of a cumulus cloud ensemble with the large-scale environment. Heating and moistening of the environment is through cumulus induced subsidence and detrainment of saturated air at cloud tops. The cloud mass flux is determined by the closure assumption that the generation of the cloud available potential energy by the large-scale flow is in quasi-equilibrium with its destruction due to clouds. The scheme used in this study is described in detail by Tiedtke (1985). It has been developed by closely following the original proposal by Arakawa and Schubert, and as further outlined by Lord et al. (1982); the exception is in the cloud physics where we simply assume that cloud water is instantaneously converted to precipitable water, which then detrains at the cloud tops, and that rain re-evaporates in sub-cloud layers as well as within the

environmental air of cloud layers. The re-evaporation of rain in cloudy layers significantly reduces the scheme's tendency to cause excessive drying of the atmosphere as noted by Lord (1982). Cumulus scale transport of horizontal momentum is disregarded in both schemes.

## 2.2 Initial conditions and forecasts

All integrations start from real data from the FGGE observing period. A starting date of 12Z 11 June 1979 was chosen so as to cover the period of explosive growth of kinetic energy of the low level flow over the Indian Ocean coinciding with the onset of the monsoon over India. This case was selected by David Baumhefner of the NCAR for numerical experiments by the many groups investigating the Asian summer monsoon.

The fields are analysed and initialised at ECMWF as described by Lorenc (1981). The data assimilation scheme is identical to that used for producing the FGGE III-b analyses with the important exception that the analysis increments are interpolated to the model coordinates and added to the first guess (a 6 hour forecast) instead of the increments being added to the first guess in pressure coordinates and the complete analysis field interpolated to the model coordinates (see Lönnberg and Shaw, 1983).

Two experiments were performed, involving three forecasts from the same starting date. In the first experiment an extended (50-day) integration was carried out using the Kuo convection scheme with the aim of assessing the model's performance over a period long enough to cover the main monsoon onset and at least one monsoon 'break'. In the second experiment two 10-day integrations were performed, one using the Kuo convection scheme (slightly modified) and the other the A-S scheme. The aim was to compare the performance of the two schemes over the period of explosive growth.

The forecasts are verified against the original FGGE III-b analysis based on full field interpolation. Differences between forecasts and analyses occur initially because of the differences in the data assimilation schemes used for model initialisation in the experiments and in the FGGE analyses.

## 3. MAIN FEATURES OF THE MODEL 50-DAY SIMULATION (KUO CONVECTION SCHEME)

It was shown in the earlier purely observational study (Pearce and Mohanty, 1984) that the major changes occur over the Arabian Sea during the monsoon onset. Time sequences of simulated means over this region (0° - 22.5°N, 41.25° - 75°E - Fig. 1) are first compared with those based on observations (Fig. 2). Comparisons are then made with observations of the simulated time-mean fields of wind, moisture and temperature for the 15-day period 16-30 June (June 2) and in less detail for the period 1-15 July (July 1) covering the region 45°S - 45°N, 0 - 180°E (Figs. 3-13). Data were extracted for the standard levels 1000, 850, 700, 500, 400, 300, 200, 150 and 100 mb. The four-dimensional data assimilation scheme, used at ECMWF to produce the level III(b) data set, is documented in detail in Bengtsson et al. (1982) and Lorenc (1981). The analysis procedures used to obtain the FGGE fields shown in Figs. 3-13 are described in Pearce and Mohanty (1984).

### 3.1 Time sequences of the total precipitable water, tropospheric mean temperature and KE of the 850 mb flow

The onset of the monsoon rains in 1979 was late, occurring over Southern India on June 11 instead of at the 'normal' time of May 31. The onset is shown up most dramatically in Fig. 2(c) (full curve) with the rapid increase of the low-level winds over the Arabian Sea. Pearce and Mohanty (1984) interpret this increase as the rapid intensification phase of a large-scale feed-back

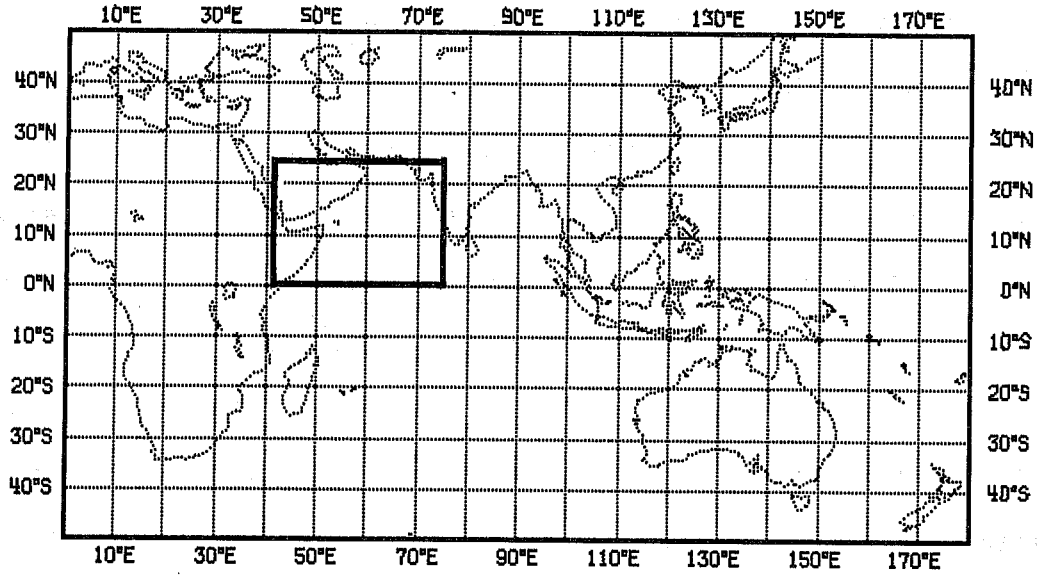


Fig. 1 The analysis area and Arabian Sea region.

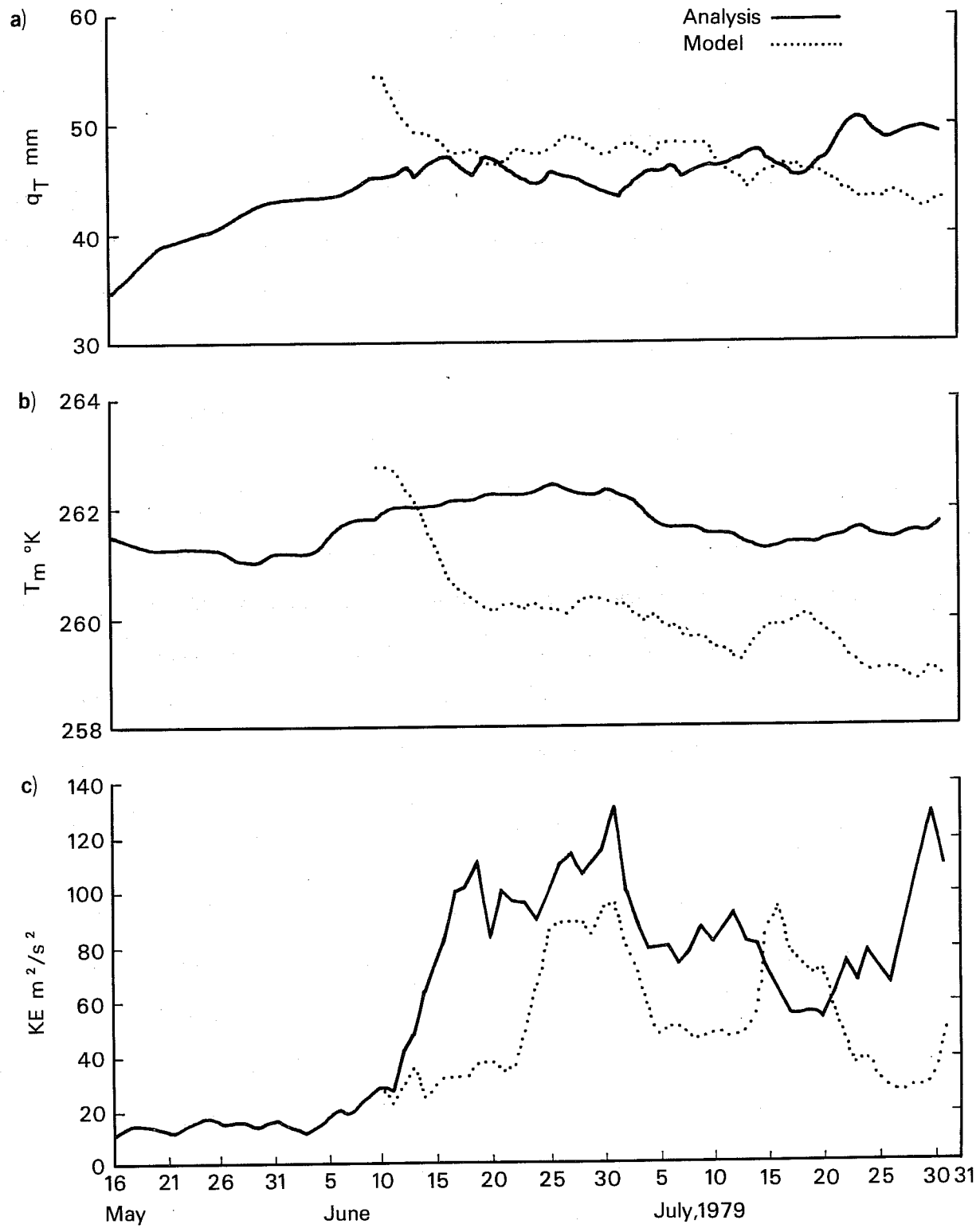


Fig. 2 Time sequences of Arabian Sea region averages of (a) total precipitable water $q_T$ (mm), (b) tropospheric (surface-100 mb) mean temperature $T_m$ (°K), and (c) kinetic energy per unit mass of the 850 mb flow ($m^2$ $s^{-2}$). FGGE III-b analyses are shown by the full curves and the model output by the dashed curves.

involving latent heat release over a large part of the Indian Ocean and organised deep moist convection over the Arabian Sea and the Indian sub-continent. This followed a moisture build-up during the latter part of May and early part of June; the June observed mean moisture levels over the Arabian Sea (around 46 mm), shown in Fig. 2(a), are generally higher than those in May (around 40 mm). The first part of June is also characterised by an increase in mean tropospheric temperature in this region from about 260 K to the level of 262 K shown in Fig. 2(b).

Now consider the behaviour of the 50 day simulation (Fig. 2, dotted line). The model starts with low-level westerly winds over the Arabian Sea and a moisture level corresponding to the end of the build-up period at the crucial stage just before the commencement of the intensification of convection over the region. The model moisture over the Arabian Sea is in fact initially higher than the observed, a feature associated with differences in the data-assimilation schemes used for the initial fields in the integrations and for the verification. The same is also true of the initial temperature.

The model fails to produce initially the intensification of the low-level winds over the region. The moisture level drops over the next 10 days to the value obtained in the FGGE data analysis; the mean tropospheric temperature also decreases to values lower than that based on the FGGE analysis. However, from June 22, the model produces a sharp intensification of the low-level wind to a value close to that reached by the atmosphere itself some 10 days earlier. At this stage the mean tropospheric temperature ceases to fall and the mean moisture content stabilises. Subsequently, the model exhibits a sharp drop in intensity of the low-level winds, followed (around July 13) by a further sharp intensification.

These model features are discussed further in Sect. 4.

### 3.2 Mean wind, moisture and temperature distribution

It is immediately clear from Fig. 3, showing the 15-day mean winds for the second half of June at 850 mb and 150 mb, that the model reproduces the main features of the observed monsoon circulation, i.e. the extensive belt of easterlies at low latitudes at 150 mb (extending across Central Africa) and the low-level easterlies across the Indian Ocean which turn northwards up the East African coast and then westwards as the monsoon south-westerlies, across the Arabian Sea and India. Closer examination, however, reveals some deficiencies:

(i) at 150 mb, there are strong north-easterlies over the Indian Ocean, over and south of the equator and over SE Asia, whereas the model flow is much more zonal; also the south-westerlies over the eastern Mediterranean, with implied divergence over North Africa, are not apparent;

(ii) at 850 mb the northerlies over Arabia are missing and the model's southerly flow off East Africa is also weaker than that observed;

(iii) at both levels, the weak winds over Central and North Africa are not reproduced.

The corresponding fields for July 1-15 are shown in Fig. 4. For this period the model reproduces well the upper level flow over the Eastern Mediterranean. However it still does not simulate the extensive cross-equatorial upper north-easterlies, neither does it reproduce the north to north-west flow over

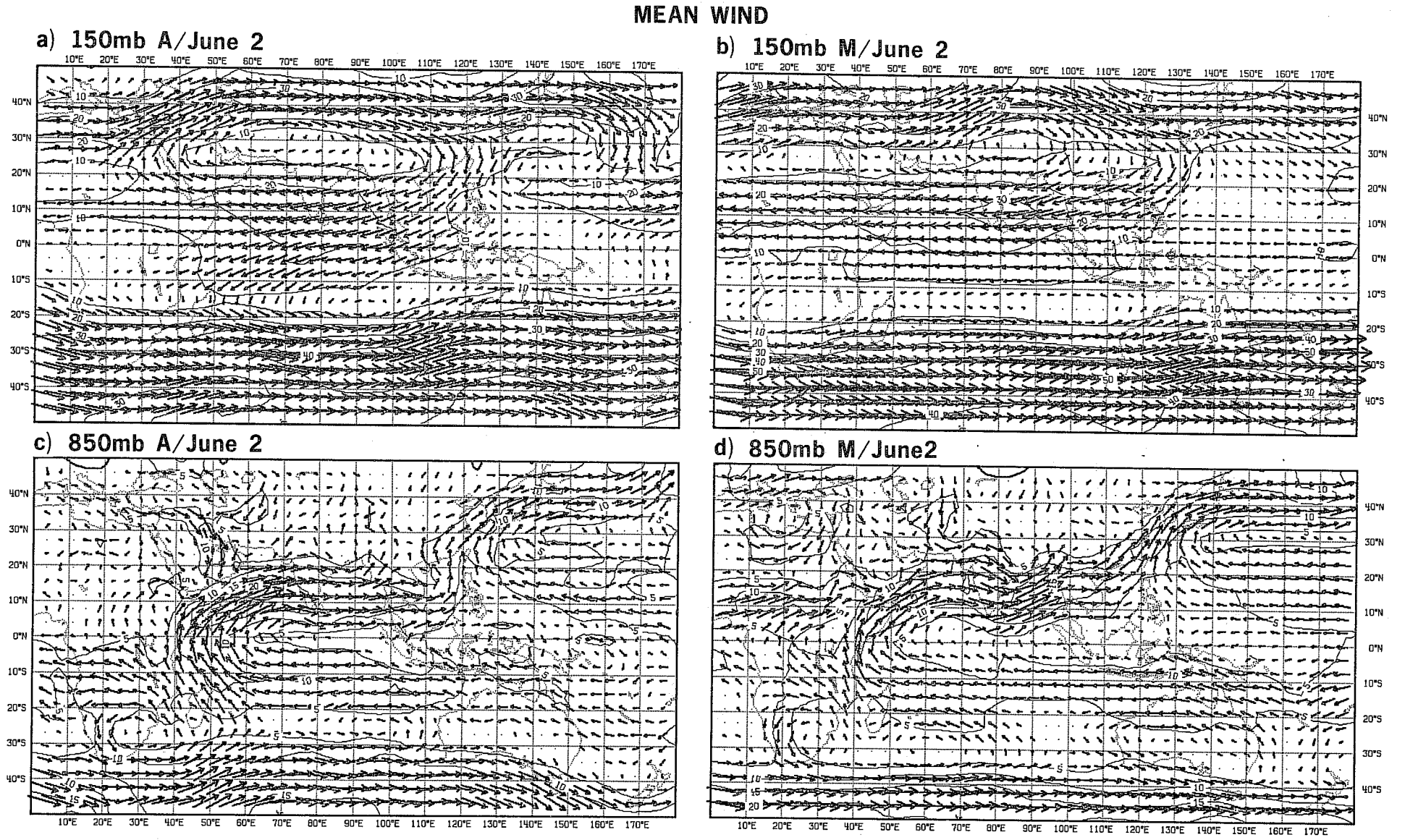


Fig. 3 Mean flow vectors and isotachs (m $s^{-1}$) for 16-30 June 1979 of (a) 150 mb winds from uninitialised FGGE III-b data, (b) 150 mb model winds, (c) 850 mb analysed winds, and (d) 850 mb model winds; 2 mm corresponds to 10 m $s^{-1}$.

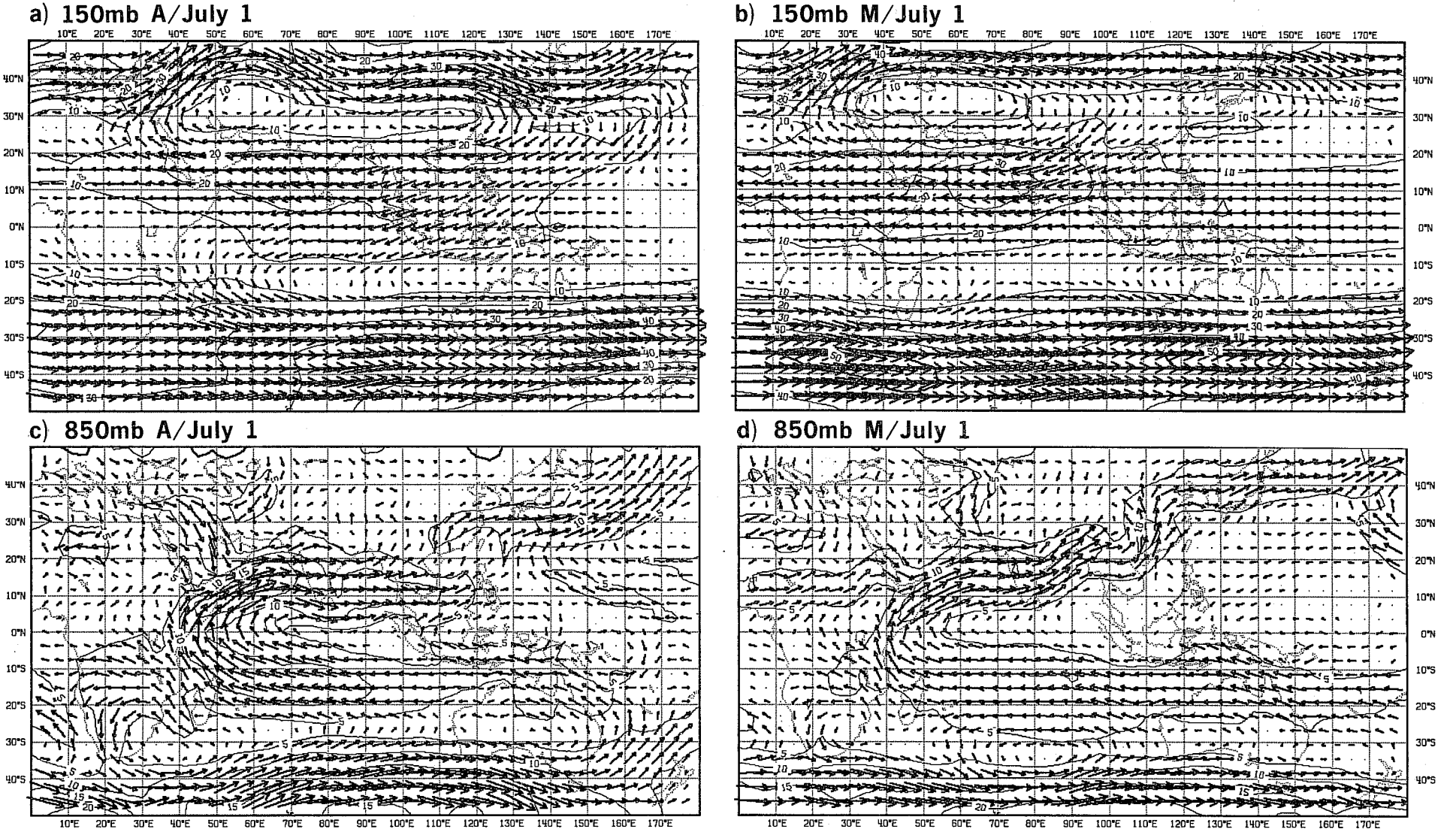


Fig. 4 As for Fig. 3, but for 1-15 July 1979.

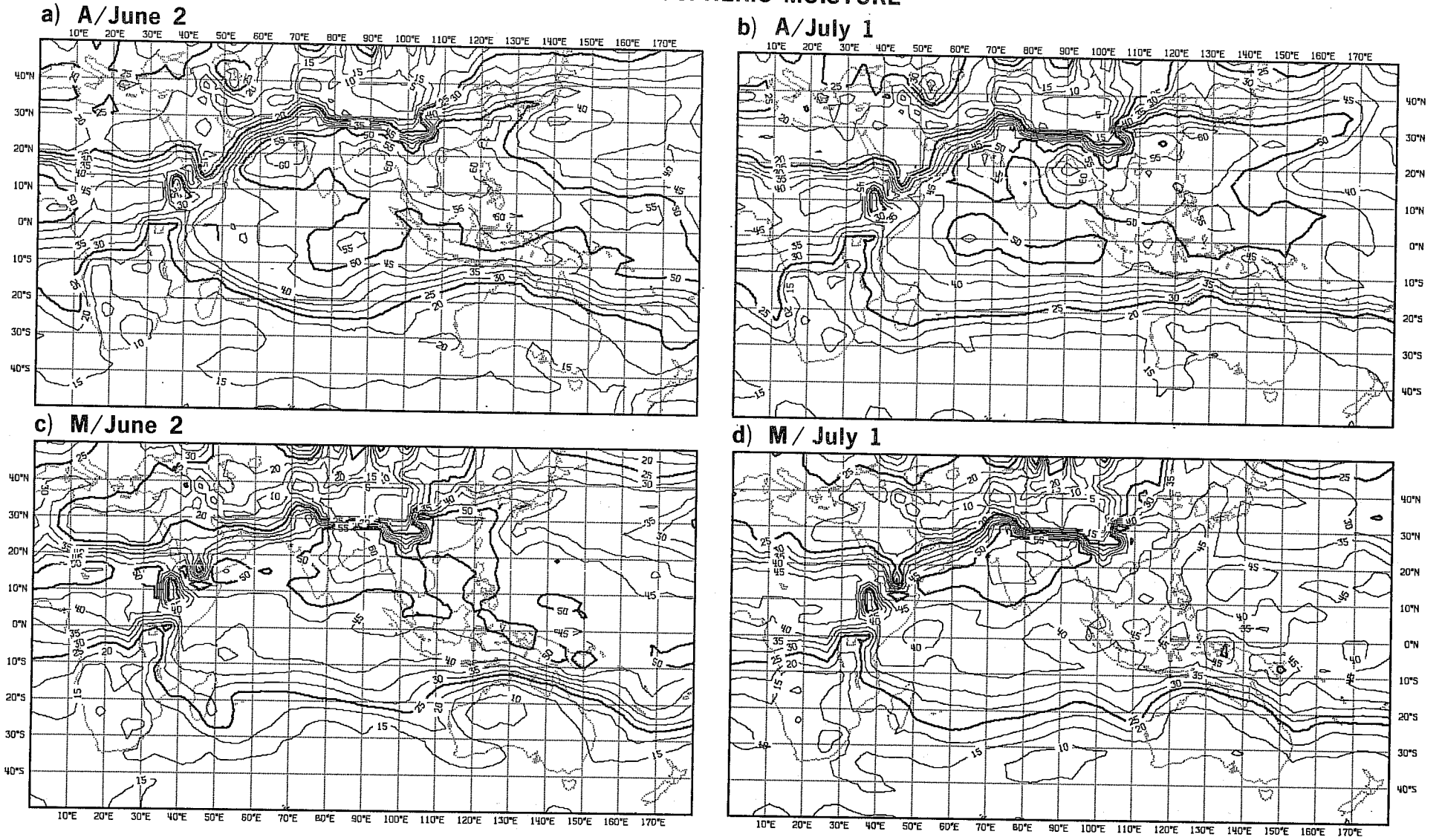


Fig. 5 Mean tropospheric moisture (precipitable water) in mm from FGGE analyses for (a) 16-30 June 1979 and (b) 1-15 July 1979. Model simulations are shown for (c) 16-30 June 1979 and (d) 1-15 July 1979.

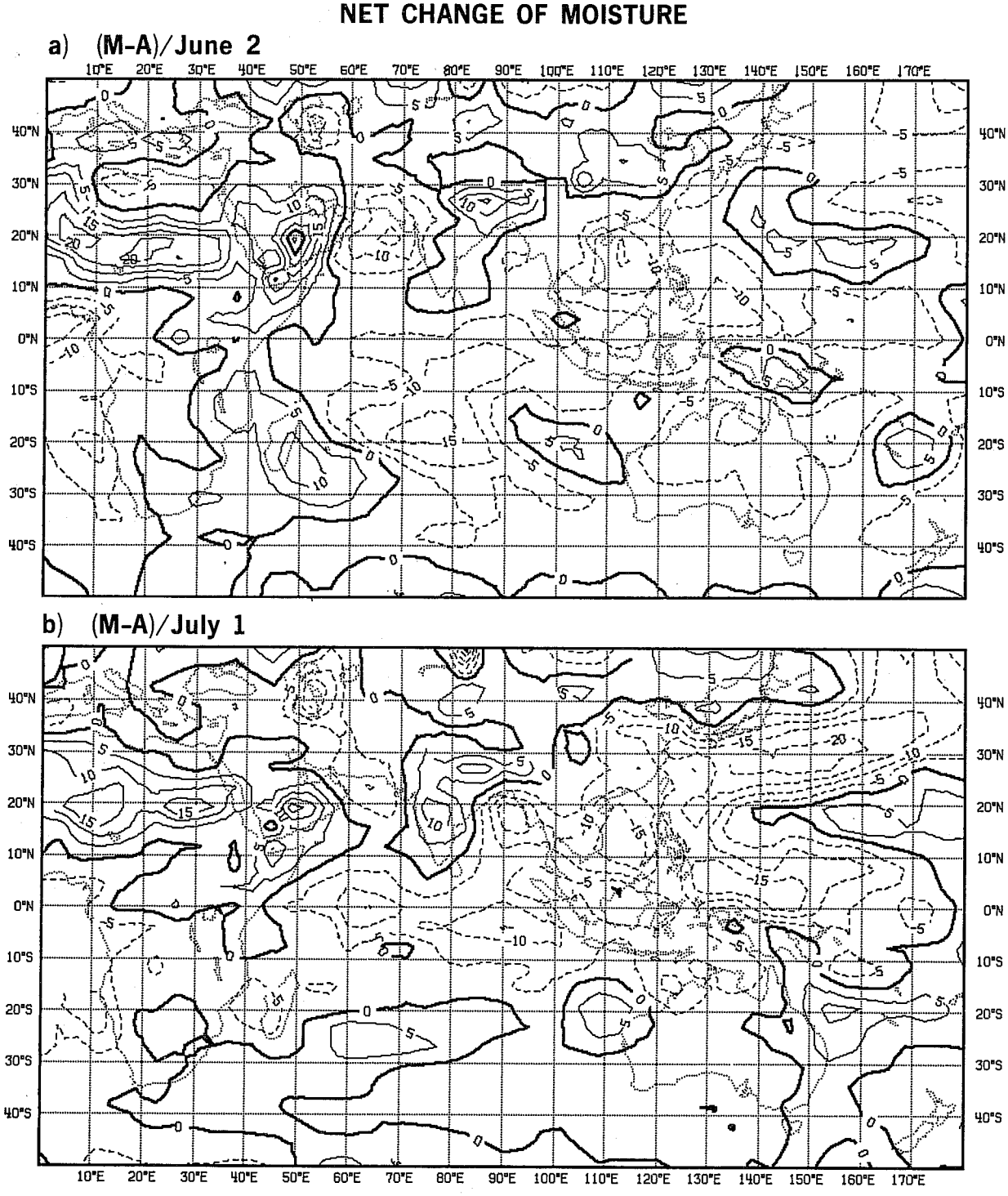


Fig. 6 Forecast error in the change of mean tropospheric moisture (precipitable water) in mm for (a) 16-30 June 1979 and (b) 1-15 July 1979.

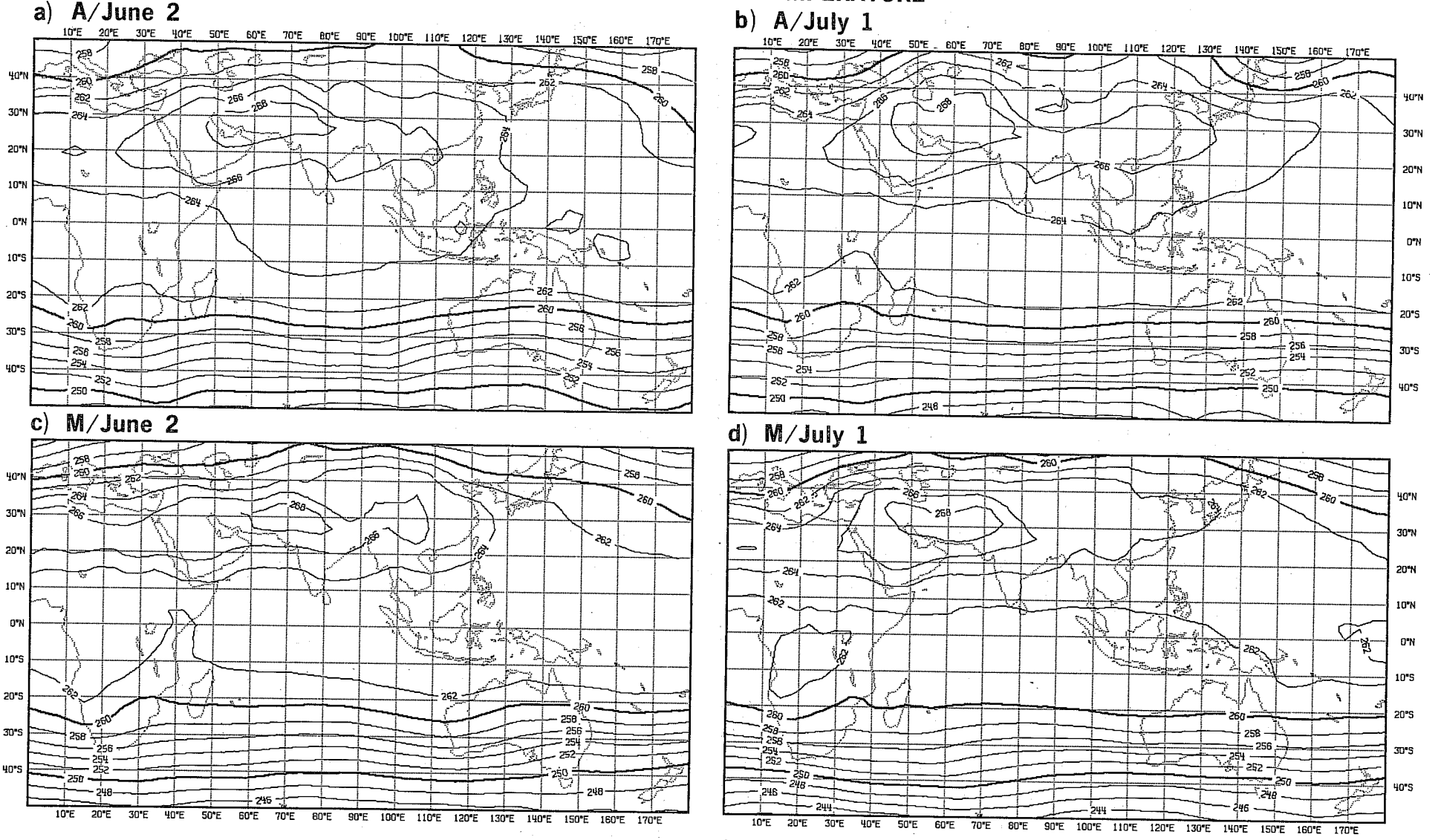


Fig. 7 Mean tropospheric temperature (surface-100 mb) in $^{o}$K for (a) 16-30 June 1979 and (b) 1-15 July 1979. Model simulations are shown for (c) 16-30 June 1979 and (d) 1-15 July 1979.

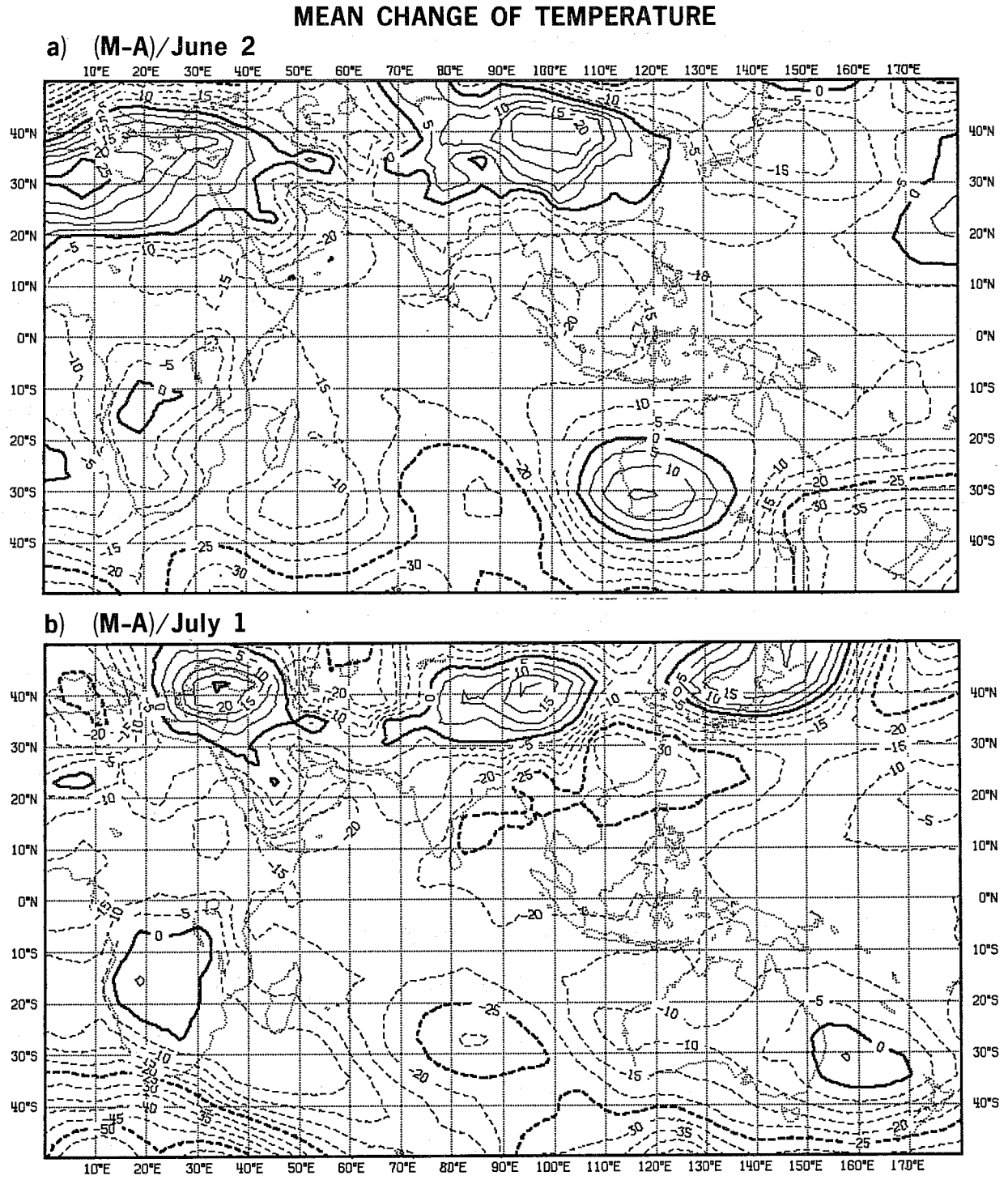


Fig. 8 Forecast error in the change of mean tropospheric temperature in $^{o}$K for (a) from 16-30 June 1979 and (b) from 1-15 July 1979.

the Indian Ocean off South Africa. There are also significant differences in the 850 mb flow, notably a generally weaker model cross-equatorial southerly off East Africa and a failure to maintain both the westerlies across the Bay of Bengal and Malaysia and the north-westerly from the Mediterranean across Saudi Arabia.

It is interesting to consider the behaviour of the model's moisture and temperature forecasts by examining the mean fields of tropospheric moisture and temperature, and their departures from the zonal mean. The model moisture distributions (Figs. 5(c),(d)) agree overall with the observed distributions (Figs. 5(a), (b)) with the highest values in a belt from the equatorial West Pacific, across South East Asia and North India to Central Africa. However, the model values over the Arabian Sea are higher than those observed, and those over the Eastern Arabian Sea lower for the June period. Those over the Sahel region of North Africa are higher than the observed for both 15-day periods. These results are supported by the moisture change forecast errors in Fig. 6; these also indicate that the model tends to dry out the atmosphere over a large part of the Eastern Indian Ocean and Indonesia.

The model tropospheric temperature distributions (Figs. 7(c),(d)) are also close to the FGGE analyses (Figs. 7(a),(b)) with the maximum (268°K) occurring over Iran. However, layer means (not shown here) indicate that for June it is about 2K too high in the lower troposphere and 2K too low at middle levels. Thus the model atmosphere is statically more unstable than the observed atmosphere in this region. The forecast temperature changes (Fig. 8) show that the model tends to cool the atmosphere below its observed value over most of the tropical belt.

### 3.3 Moisture and enthalpy budgets

It is interesting to compare the net moisture fluxes in the model with those inferred from FGGE data; these fields are shown in Fig. 9. As is to be expected, over the oceans this flux closely resembles the 850 mb flow and so the accuracy of the model simulation depends upon how well the low-level flow is reproduced. The model clearly transports too much moisture eastwards across Africa near 10°N.

The moisture and enthalpy budget equations for an atmospheric column may be approximated as

$$\overline{\nabla\cdot(\underline{v}q)} \cong E - P \qquad (1)$$

$$\overline{\nabla\cdot(\underline{v}T)} - \frac{\overline{\omega\alpha}}{c_p} \cong \frac{\bar{Q}}{c_p} \qquad (2)$$

using standard notation (the bars denoting averages from the surface to 100 mb). The neglected terms are time derivatives and vertical fluxes at the surface and 100 mb.

Vertical motion ($\omega$) fields were obtained using a version of O'Brien's kinematic method (see Pearce and Mohanty, 1984 for details) and the terms on the left of equations (1) and (2) computed directly. The column diabatic heating $\bar{Q}$ was then obtained as a residual. There are strong correlations between the terms in these equations and these are summarised in Table 1.

Table 1

Signs of dominant terms in moisture and heat budget equations

| | $\overline{\nabla\cdot(\underline{v}q)}$ | $E - P$ | $\overline{\nabla\cdot(\underline{v}T)}$ | $\bar{Q}$ | $\overline{\omega\alpha}$ |
|---|---|---|---|---|---|
| $\bar{\omega} > 0$ | + | + | + | (-) | + |
| $\bar{\omega} < 0$ | - | - | - | + | - |

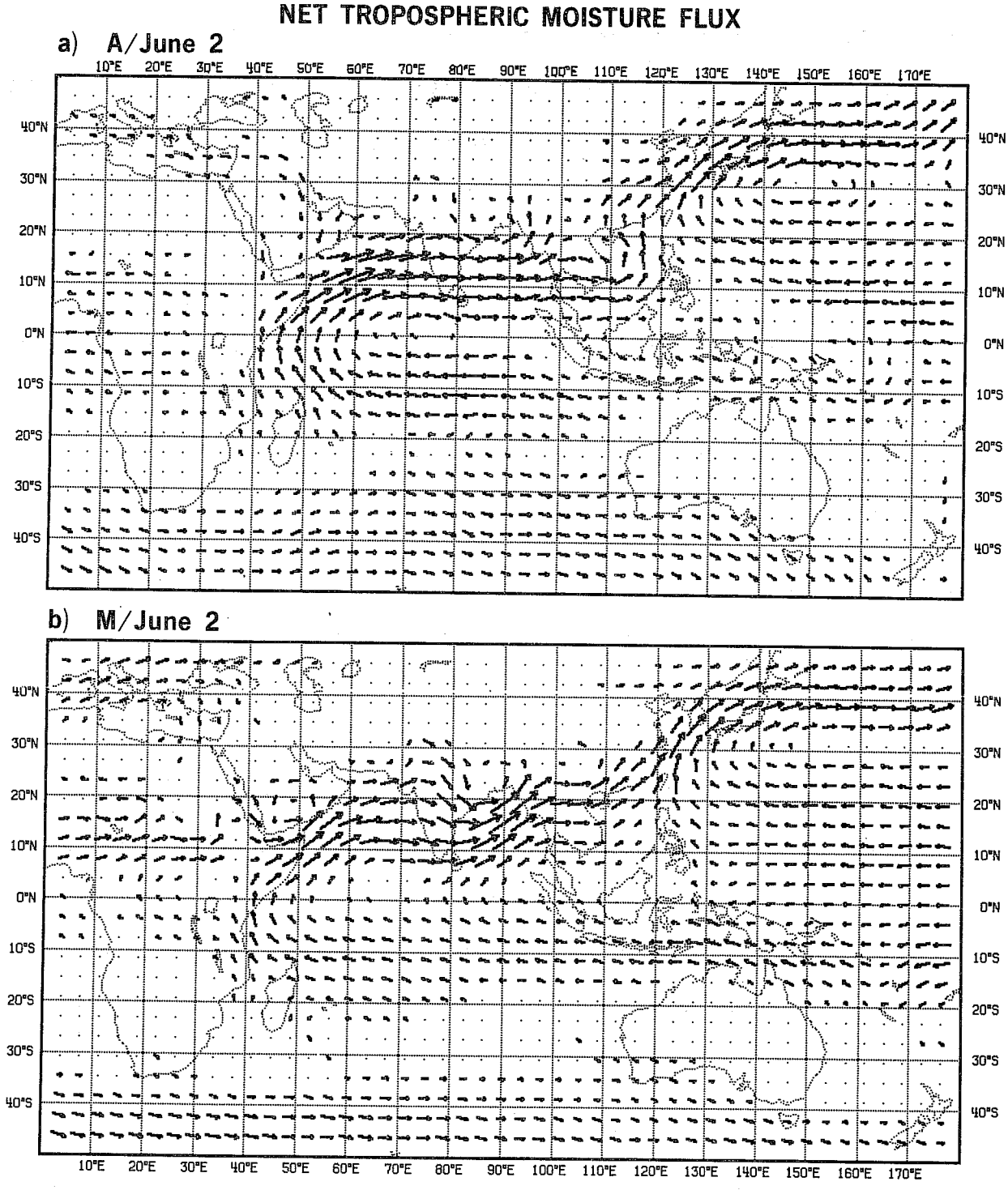


Fig. 9 Mean vectors for 16-30 June 1979 of (a) net tropospheric moisture flux and (b) model simulation of (a).

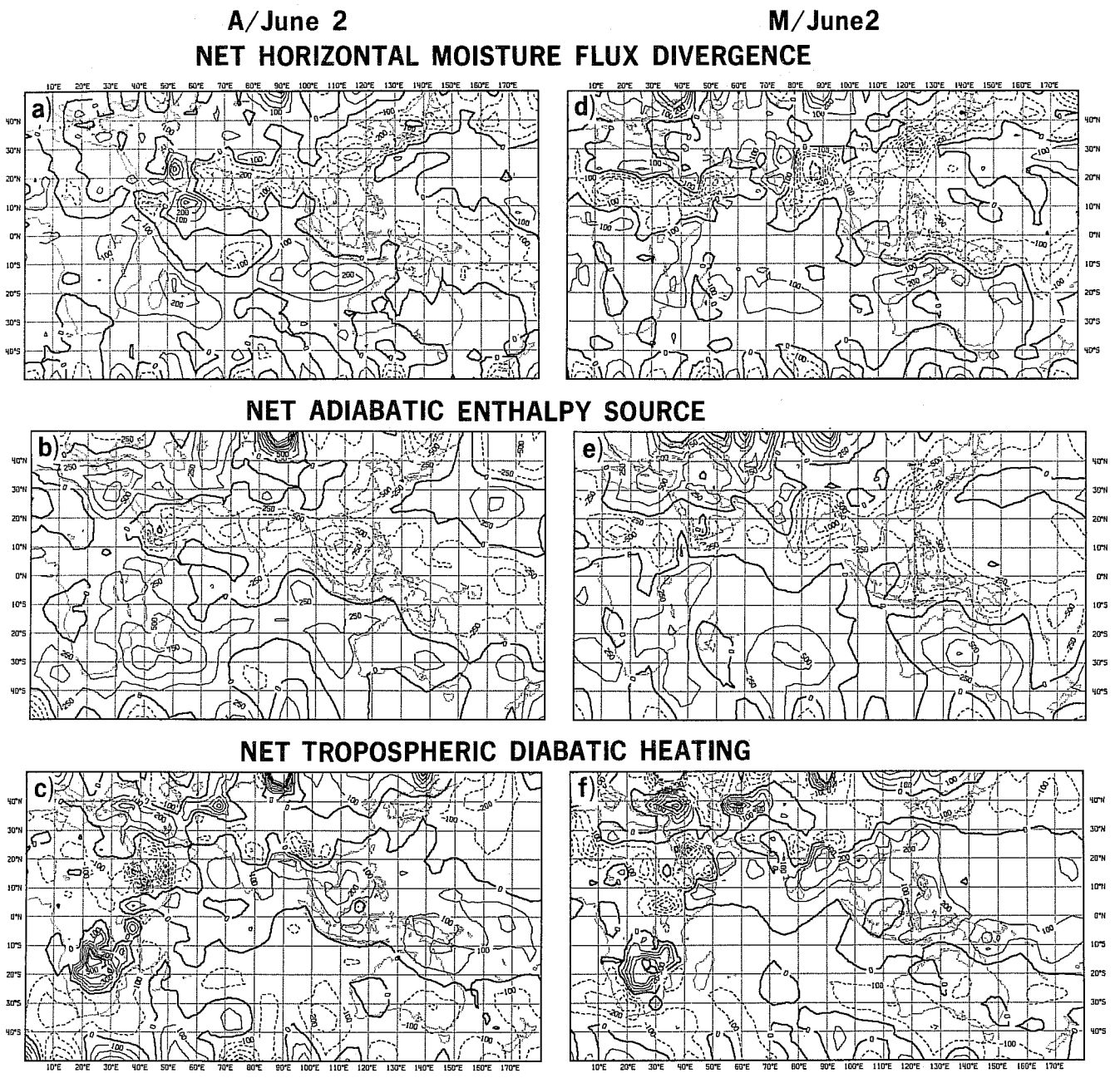


Fig. 10 Mean fields of FGGE analyses for 16-30 June 1979 in W $m^{-2}$ of (a) horizontal flux divergence of latent heat, (b) tropospheric adiabatic enthalpy source ($\widehat{\omega\alpha}$) and (c) net tropospheric heating. (d), (e) and (f) are model simulations of (a), (b) and (c) respectively. Full lines denote positive values, dashed lines negative.

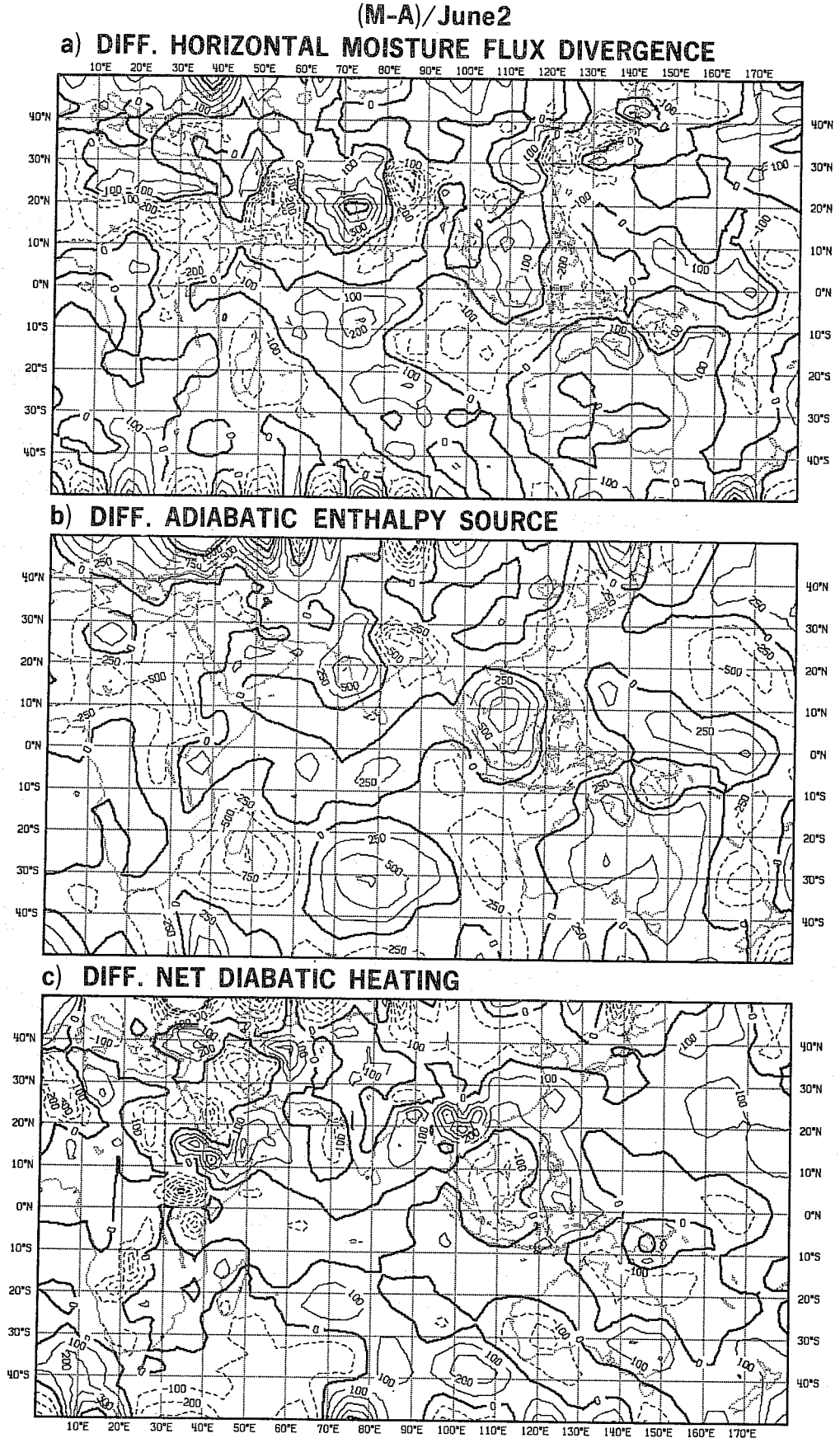


Fig. 11 Forecast error fields of the changes between 16-30 June 1979 of (a) horizontal flux divergence of latent heat, (b) tropospheric adiabatic enthalpy source ($\widehat{\omega\alpha}$) and (c) net tropospheric heating. Full lines denote positive values, dashed lines negative.

Figs. 10 and 11 enable comparisons to be made of the model and analysed fields for the June period of quantities entering the moisture budget equations, i.e. derivatives of moisture and flow fields; these constitute a stricter test than a comparison of the mean moisture fields. The fields broadly agree over South East Asia and the West Pacific, but exhibit differences over Africa, the Arabian Sea and the Iran/Pakistan region. The model moisture convergence (Fig. 10(d)) is larger over the north Bay of Bengal than the analysed value (Fig. 10(a)) and there is divergence in the model fields over North West India, where there is convergence in the analysed fields. On the other hand the analysed divergence over the west Arabian Sea is not reproduced in the model - neither is that near Madagascar. The model convergence over North Africa is also not present in the analyses. The forecast error fields for the period (Fig. 11(a)) quantify these differences. As is to be expected with these second-order quantities, the forecast errors are generally of the same order as the fields themselves; where sign differences occur, as in the regions quoted, they are larger.

The other fields shown in Figs. 10 and 11 show features consistent with those of the moisture flux divergence as indicated in Table 1. The enthalpy source (essentially a weighted mean of $\omega$) has broadly the same sign as the moisture flux divergence, and the diabatic heating the opposite sign. The regions of ascent over the northern Indian Ocean and west Pacific are clearly evident in Figs. 10(b) and 11(b); the larger than observed model values over Bangladesh and Central Africa are particularly noticeable. FGGE and model moisture sources and sinks involving both latent heat releases and surface fluxes have been computed but are not reproduced here. These show large discrepancies over the same part of Africa and also over the Arabian Sea; the model surface fluxes over the eastern part of the Arabian Sea (associated with the local subsidence over North West India - cf. Fig. 10(e)) are too large; the net source off Somalia is too small.

The area of strong subsidence over Madagascar (Fig. 10(b)) is not present in the model (Fig. 10(e), although there is strong subsidence about 30° further to the east. The model net tropospheric heating agrees reasonably well with the FGGE analyses (Figs. 10(c) and (f)) apart from over North Africa and Indonesia where a model maximum occurs on the equator at 130°E; also the model gives rather larger values than the analysed ones over the north Bay of Bengal and South East Asia. In mid-latitudes, poleward of 30°, many of the discrepancies must be associated with the neglect of the eddies, i.e. of $\nabla\cdot(\overline{\underline{v}'q'})$ and $c_p\nabla\cdot(\overline{\underline{v}'T'})$, and should be ignored.

### 3.4 Meridional-height cross-sections (Arabian Sea and Bay of Bengal)

The Arabian Sea and the Bay of Bengal with its adjacent land areas are of particular significance in monsoon studies since they are where the main monsoon rainfall and latent heat release occur. Fig. 12 shows 15-day means of regional zonal averages of meridional wind (v), zonal wind (u), relative vorticity ($\zeta$) and vertical motion ($\omega$) for the Arabian Sea.

Although the fields produced by the model exhibit the same general features as the FGGE analyses, there are some significant differences. For the Arabian Sea these are:

(i) The model upper tropospheric northerly components (Fig. 13(a), dashed curves) are less intense and less extensive than those in the FGGE analyses (Fig. 12(a)), particularly in the Southern Hemisphere. (The difference during the first half of July, not shown here, is even more pronounced). The weak return flow in the upper troposphere is characteristic of the model's simulation of a monsoon which is weaker than observed.

(ii) The model monsoon westerlies 0° - 15°N (Fig. 13(b)) generally do not extend as far upwards as those observed (Fig. 12(b)).

(iii) The model vorticities (Fig. 13(c)), particularly at low levels near 10°N, are less than the FGGE analysis values (Fig. 12(c)).

(iv) The model ascent between 10°N and 20°N, although of approximately the right magnitude (Fig. 13(d), dashed curves) is concentrated at much too high a level (although a second maximum occurs at around 800 mb in the July period - not shown).

Similar cross-sections were computed for the Bay of Bengal, but are not shown here. The dominating difference during the June period is in the vertical motion, the model ascent in the Northern Hemisphere and descent in the Southern Hemisphere being much more intense than the values from the FGGE analyses - a reflection of the much higher level of convective activity in the model over Bangladesh and the north Bay of Bengal as already noted (Figs.11(b),(c) near 20°N 90°E).

## 4. COMPARISON OF 10 DAY MODEL SIMULATIONS USING THE KUO AND ARAKAWA-SCHUBERT (A-S) CONVECTION SCHEMES

The Kuo and the A-S schemes have previously been compared in simulations of the atmospheric general circulation (Tiedtke, 1984). Both schemes produced similar heating rates and a similar planetary scale mean flow. However, noticeable differences occurred over the Indian Ocean, where the A-S scheme gave significantly larger heating rates connected with a more intense convergent flow.

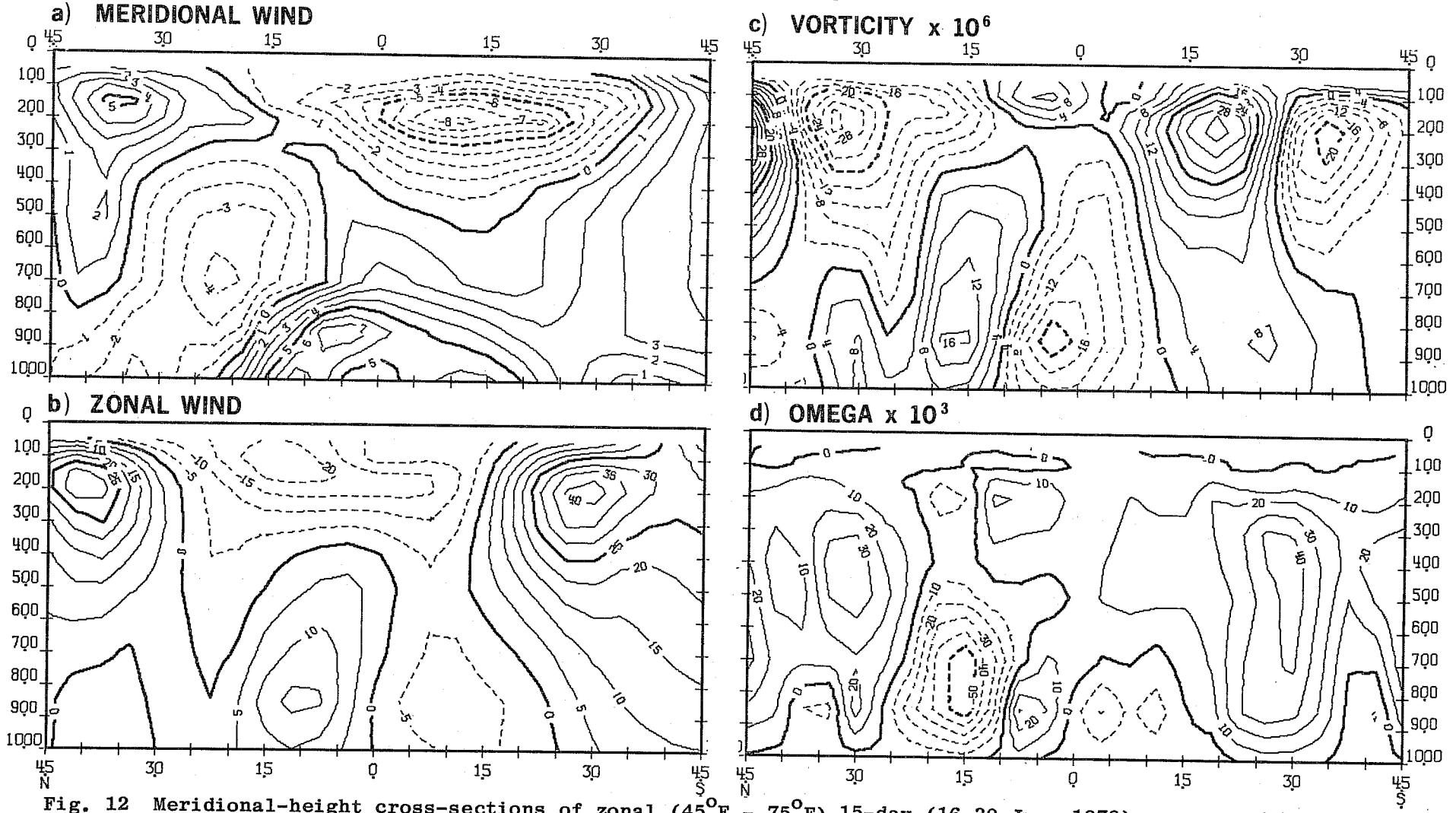


Fig. 12 Meridional-height cross-sections of zonal (45°E - 75°E) 15-day (16-30 June 1979) means of (a) southerly wind component (v) in m $s^{-1}$, (b) westerly wind component (u) in m $s^{-1}$, (c) relative vorticity ($\zeta$) in $10^{-5}$ $s^{-1}$, (d) vertical motion ($\omega$) in $10^{-3}$ Pa $s^{-1}$ - approx. mb $day^{-1}$. Full lines positive values, dashed negative.

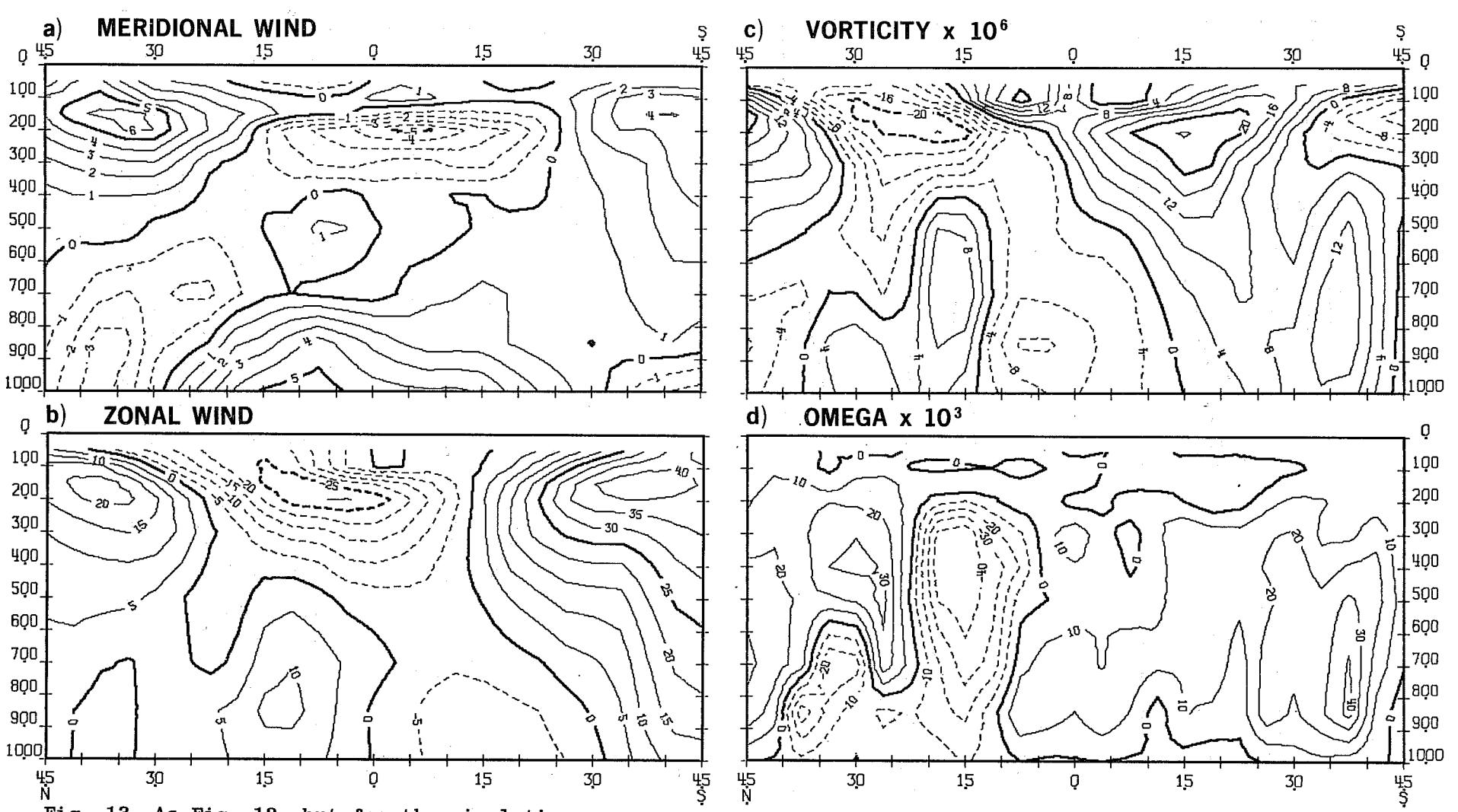


Fig. 13 As Fig. 12, but for the simulation.

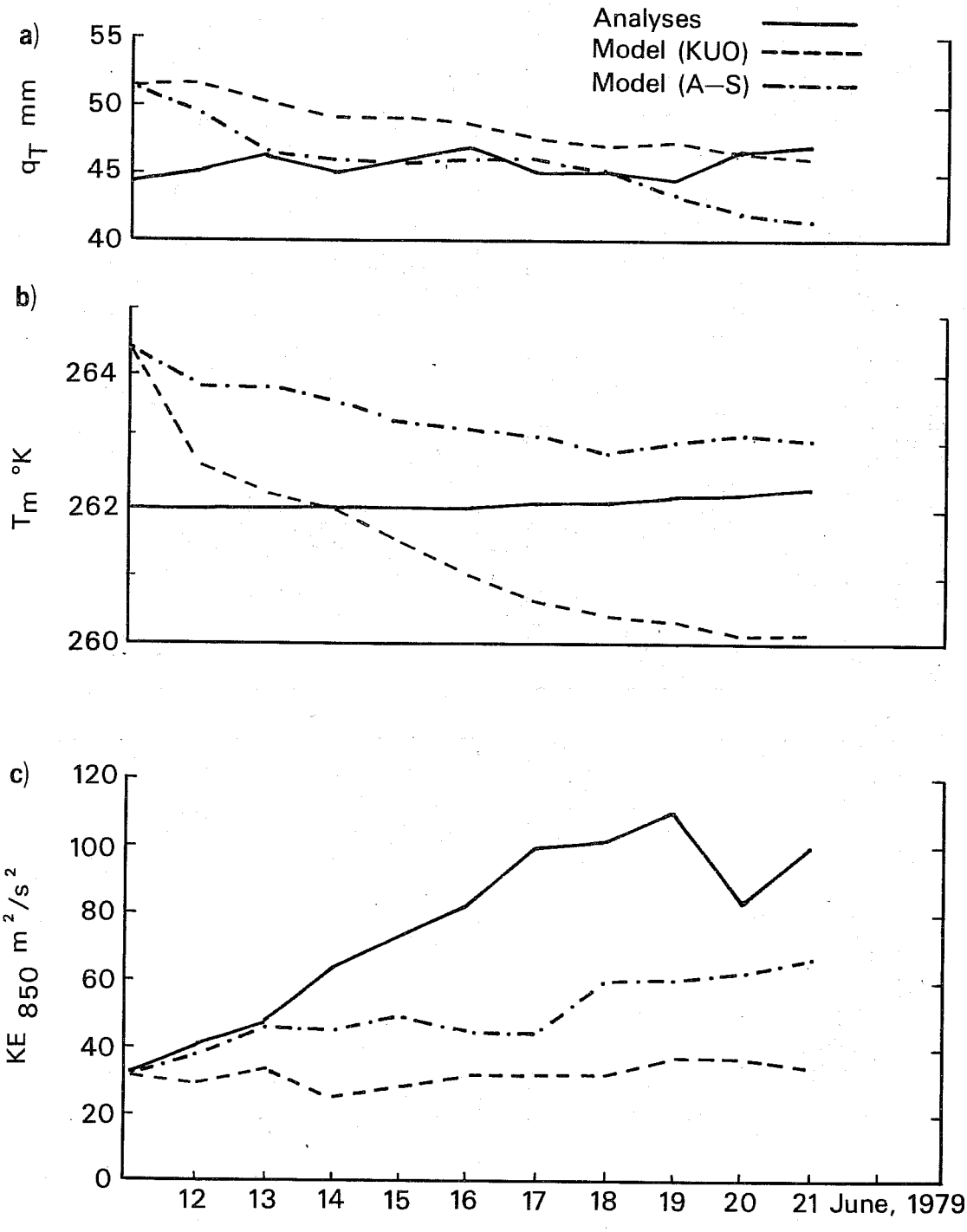


Fig. 14 Time sequences of Arabian Sea region averages of (a) total precipitable moisture (mm), (b) tropospheric mean temperature ($^{o}$K), and (c) kinetic energy per unit mass of 850 mb flow ($m^2$ $s^{-2}$). Full curves refer to FGGE III-b analysis, dashed curve Kuo scheme and dash-dot curve A-S scheme.

## 4.1 Arabian Sea time-sequences

Fig. 14 shows the time evolution of the area mean values of q, T and kinetic energy for the FGGE analyses, the simulation with the Kuo scheme and the simulation with the A-S scheme. The A-S scheme clearly performs better than the Kuo scheme in each of these comparisons. From 13 June the moisture values are very close to the FGGE analyses until 19 June. The A-S scheme still does not produce enough heating, but the temperatures tend to drop much less than with the Kuo scheme. However the A-S scheme still fails to produce the observed intensification of the 850 mb winds.

## 4.2 Mean wind, moisture and temperature distributions

As is to be expected, the FGGE 10-day average and the corresponding results using the Kuo scheme closely resemble the 15-day averages obtained from the 50-day simulations. The A-S scheme winds are very similar to those obtained using the Kuo scheme and exhibit generally similar differences from the FGGE analyses. Fig. 15 shows the differences between the 10-day means of the forecast and analysed winds ((a)-(d)) and also the differences between the two forecasts. At 150 mb, neither forecast maintains the upper trough over the east Mediterranean, both allowing it to move eastwards. Each also fails to intensify the equatorial Indian Ocean north-easterlies and the A-S scheme produces too strong a subtropical jet over the Southern Indian Ocean. At 850 mb the A-S scheme exhibits the same model features over North Africa as the Kuo scheme. Although producing a stronger monsoonal flow over the Arabian Sea, it does not quite succeed in reproducing the full strength and extent of the analysed cross-equatorial flow off East Africa. However the differences from the analysed winds are less pronounced here in the A-S simulation.

The A-S moisture simulation over the Arabian Sea is similarly nearer the analysed distributions than that obtained using the Kuo scheme (Fig.16), although it is generally too dry there and too moist over Saudi-Arabia.

However the A-S scheme does not succeed as well as the Kuo scheme in the Southern Indian Ocean around 80°E, south of where a local maximum occurs in the analysed fields (see Fig.5(a)). (Interestingly, moisture distributions obtained for June 1982 using ECMWF operational analyses - see Pearce and Mohanty (1984) - show a similar local maximum in this region.)

The A-S tropospheric-mean temperature distribution, like the Kuo simulation, agrees well with the FGGE analyses in that the maximum is well placed over the Iran-South Arabia region; however it is about 2K too high. The forecast errors shown in Figs.17(a) and (b) are interesting. These indicate that whereas the Kuo scheme produces temperatures which are too high over the land and too low over the ocean, the A-S forecasts are rather too high everywhere. The difference between the two forecasts (Fig.17(e)) reinforce this point.

### 4.3 Moisture and enthalpy budgets

Moisture transport vectors computed using the A-S scheme (not reproduced here) are remarkably close to those inferred from the FGGE data and do not exhibit the differences obtained in both the 10-day and 50-day simulations using the Kuo scheme.

The model simulations of the moisture and enthalpy are readily related to the mean vertical motion fields, the forecast errors of which are essentially shown in Fig. 18. The forecast errors for the Indian Ocean are broadly similar, with subsidence instead of ascent over much of the Arabian Sea (cf. Figs. 10(b) and 11(b)) and ascent over northern India. The A-S simulation,

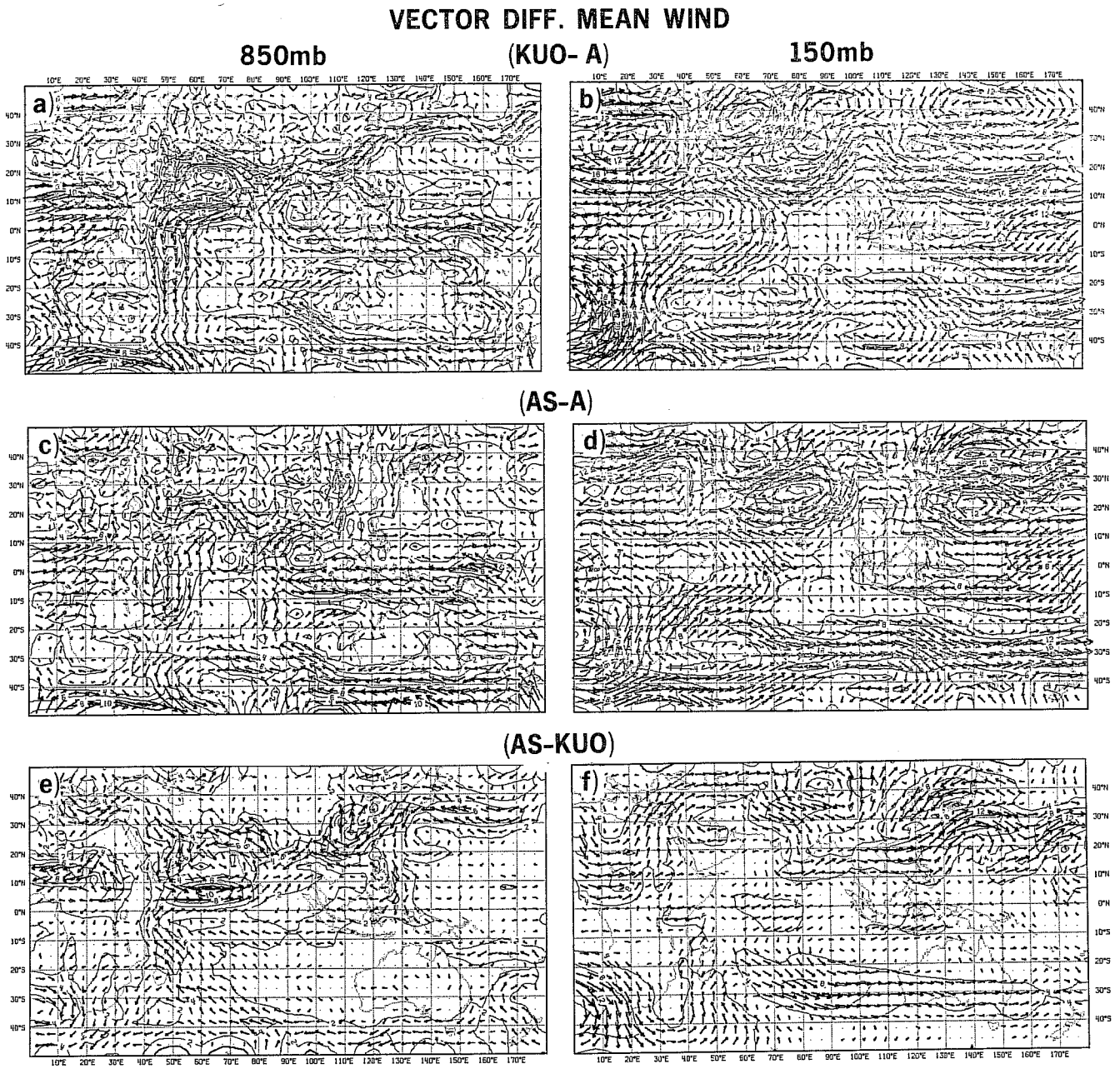


Fig. 15 Forecast error mean flow vectors and isotachs (m $s^{-1}$) 12-21 June 1979 for (a) Kuo-simulation 850 mb, (b) Kuo-simulation 150 mb, (c) A-S simulation 850 mb and (d) A-S simulation 150 mb; also differences between forecasts (A-S minus Kuo) for (e) 850 mb and (f) 150 mb.

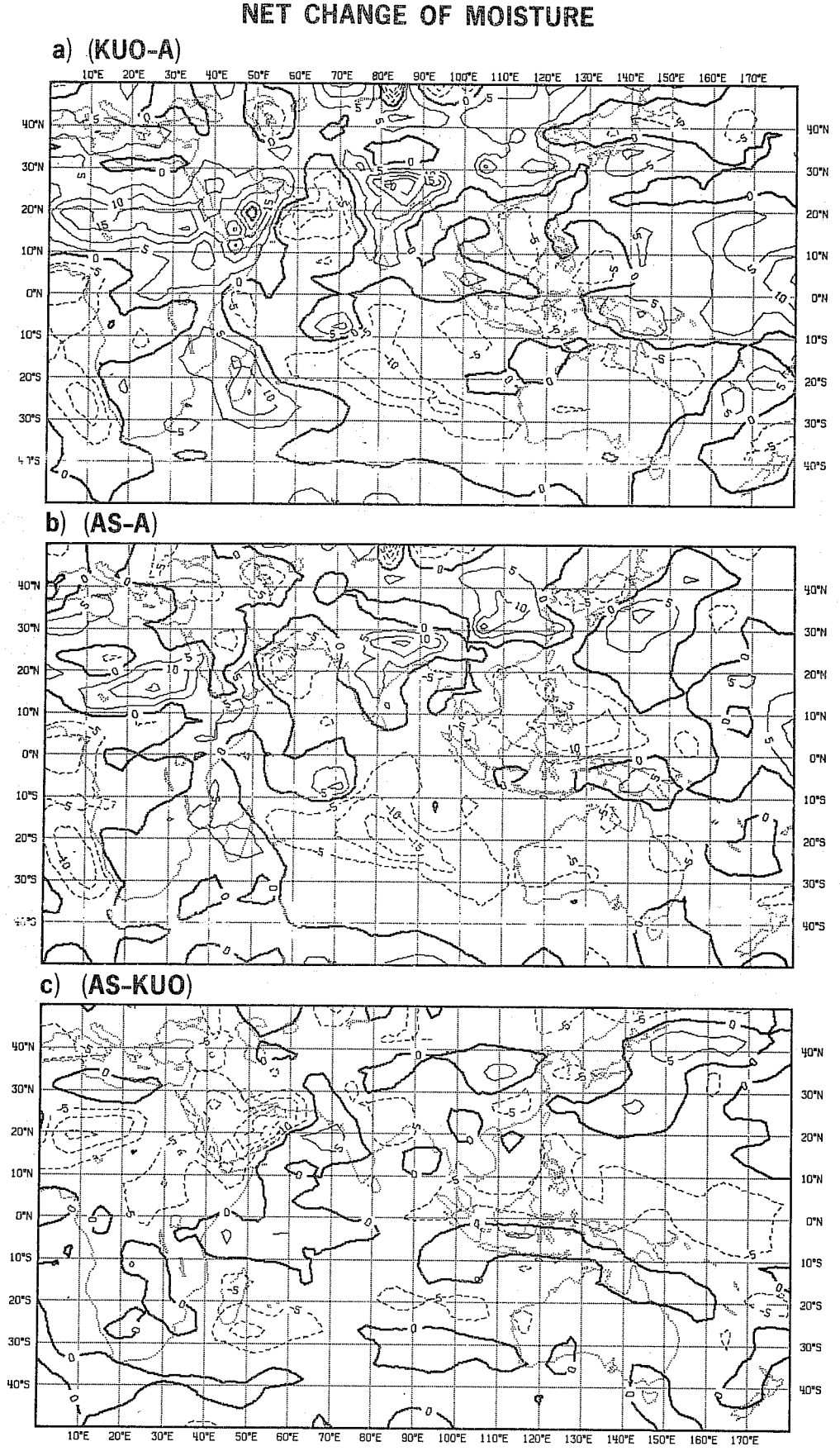


Fig. 16 Forecast error change of total moisture (mm) from 12-21 June 1979 (a) Kuo simulation and (b) A-S simulation; also (c) difference between forecasts (A-S minus Kuo).

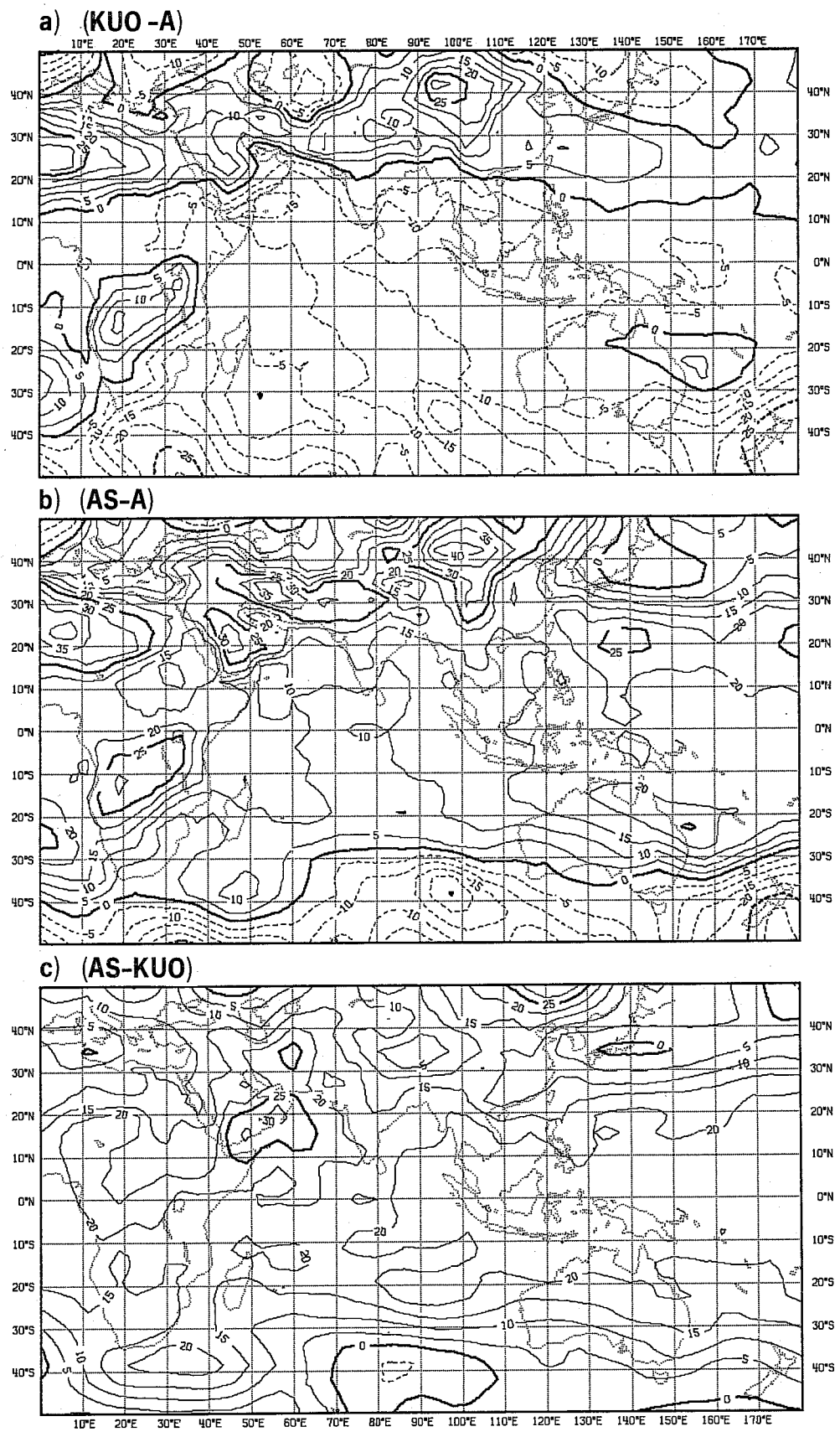


Fig. 17 Forecast error change of tropospheric mean temperature from 12-21 June 1979 (a) Kuo simulation and (b) A-S simulation; also (c) difference between forecasts (A-S minus Kuo).

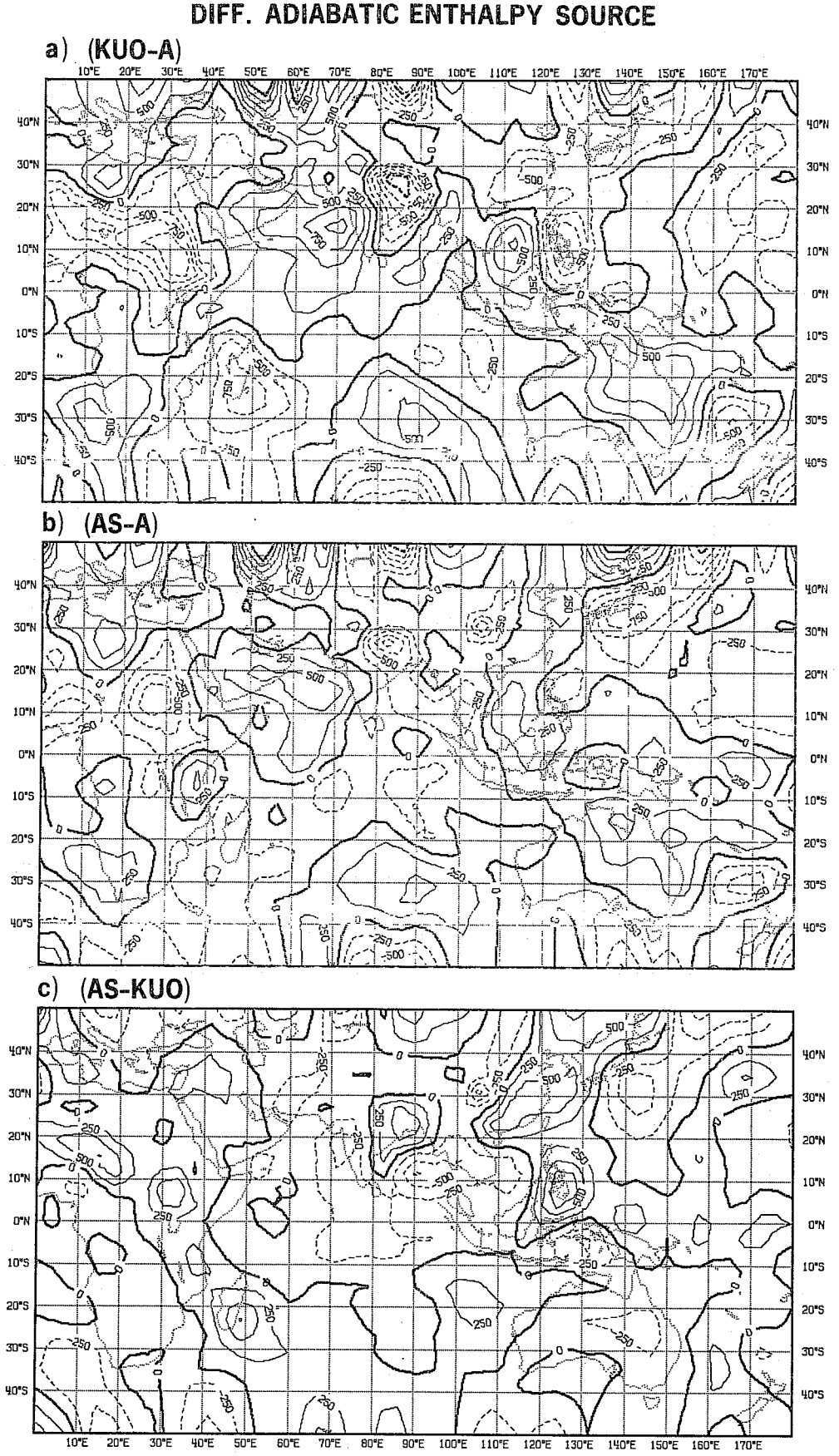


Fig. 18 Forecast error fields of mean tropospheric adiabatic enthalpy source ($\widehat{\omega\alpha}$) in W $m^{-2}$ for 12-21 June 1979 (a) for Kuo simulation and (b) for A-S simulation; also (c) difference between forecasts (A-S minus Kuo).

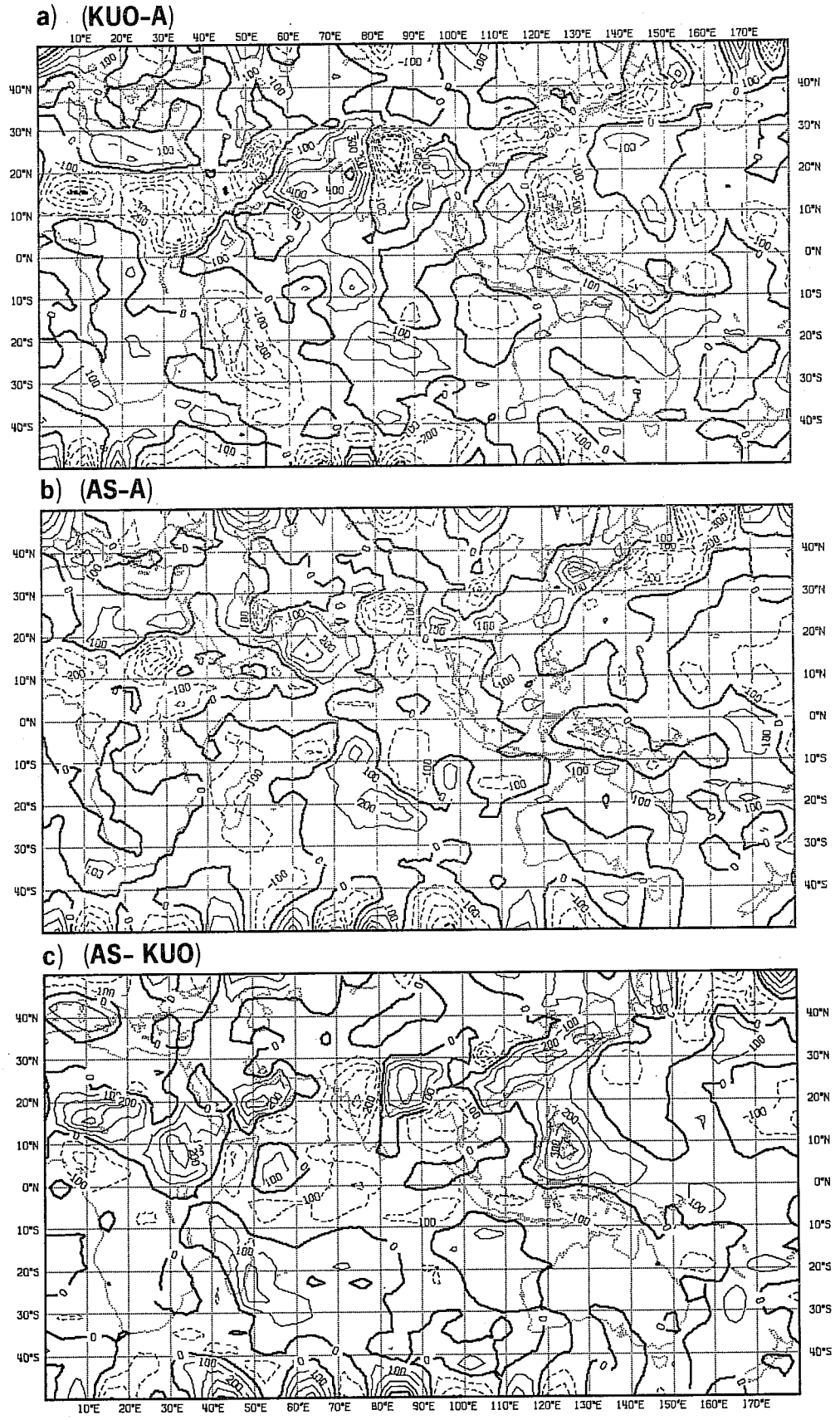


Fig. 19 Forecast error fields of horizontal flux divergence of latent heat in W $m^{-2}$ for 12-21 June 1979 (a) for Kuo simulation and (b) for A-S simulation; also (c) difference between forecasts (A-S minus Kuo).

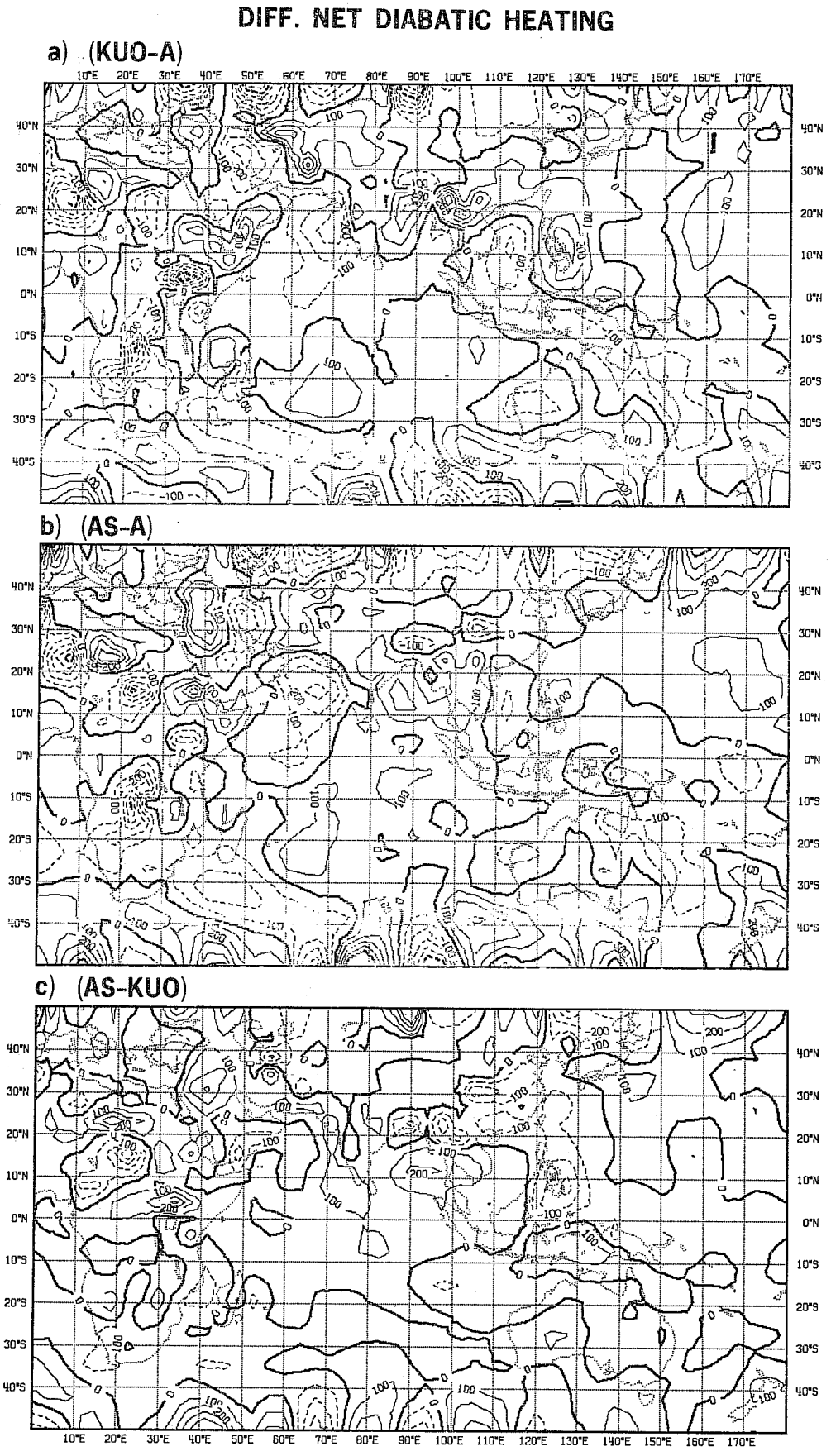


Fig. 20 Forecast error fields of net tropospheric heating in W $m^{-2}$ for 12-21 June 1979 (a) for Kuo simulation and (b) for A-S simulation; also (c) difference between forecasts (A-S minus Kuo).

however, differs less from the FGGE analyses than the Kuo simulation.

The more satisfactory treatment of the moisture by the A-S scheme is demonstrated in the analyses of the net tropospheric moisture divergence (Fig. 19). Although the Arabian Sea convergence is not properly simulated by either model, the large values of divergence present over West India in the Kuo simulation do not appear in the A-S simulation. The moisture source-sink distributions for the 700-400 mb layer (not reproduced here) also demonstrate the greater realism of the A-S fields. In particular, the rates of ascent over Bangladesh, and consequent values of the vertical moisture flux convergence and latent heat release, are much less intense and nearer the analysed values in the A-S simulation than in the Kuo simulation.

The main discrepancies in both simulations of the heating (Fig. 20) are the area of weak subsidence over the Arabian Sea and ascent over North Africa near 30°E. They are, however, more pronounced in the Kuo simulations. The A-S heating distributions is quite close to the FGGE data analysis over the near-equatorial ocean belt (Fig. 20(c)). In particular it does not produce an excessive heat source over the Philippines as does the Kuo simulation.

### 4.4. Meridional-height cross-sections

Although the 10-day FGGE (day 1 to day 10) means of u, v, $\zeta$ and $\omega$ (Figs. 21,22) are very similar to the 15-day (day 6 to day 10) means for 16-30 June 1979 (Fig. 12), the Kuo simulations show interesting differences - for example, the extension to the surface of Southern Hemisphere northerlies (compare Fig. 21(c) with Fig. 13(a)) and the strength of the low level westerly jet over the Arabian Sea (compare Fig. 21(d) with Fig. 13(b)); also the Northern Hemisphere monsoon ascent is much weaker in the 10-day mean than in the 15-day mean (compare Fig. 22(d) with Fig. 13(d)). These differences

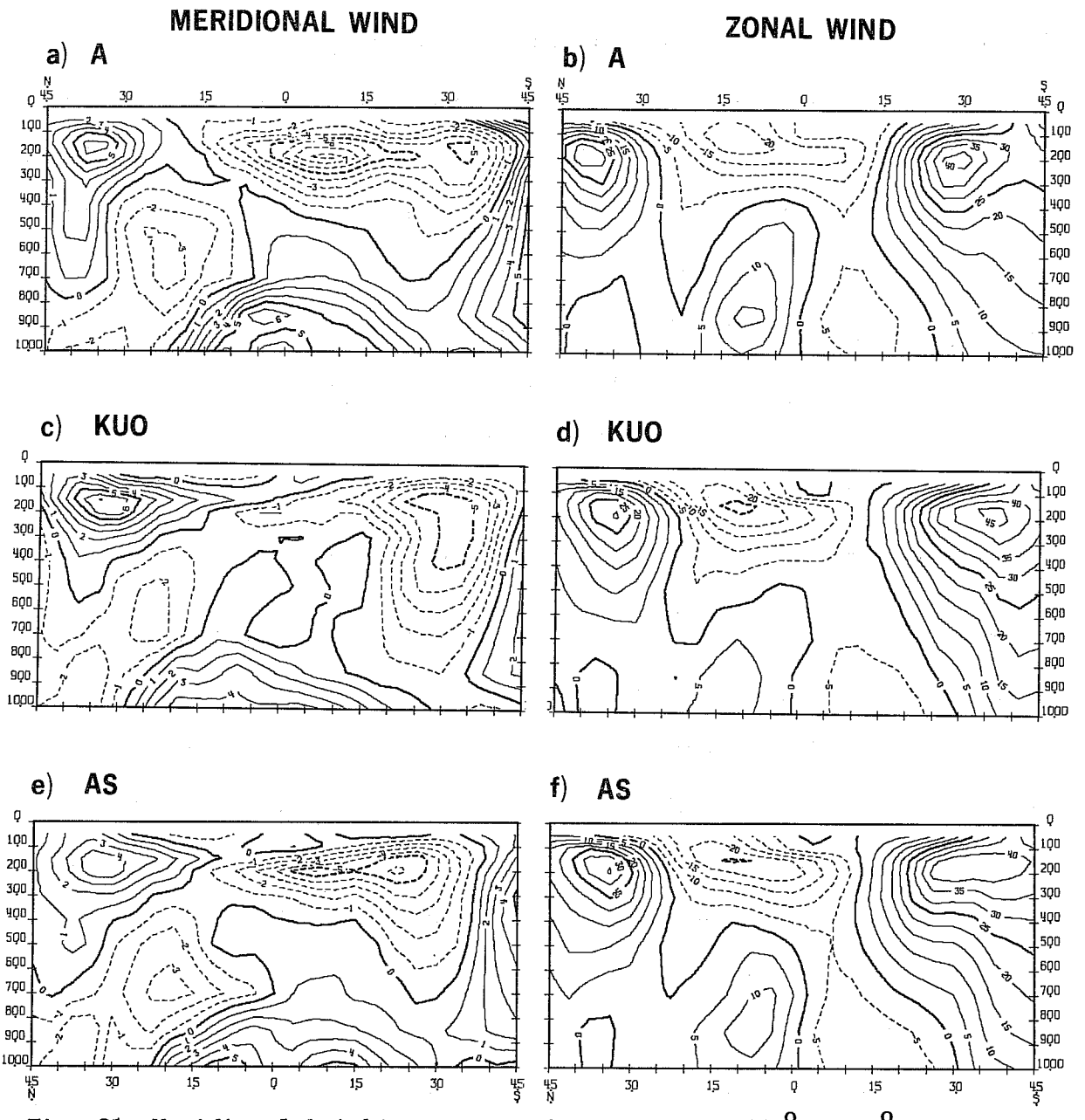


Fig. 21 Meridional height cross-sections of zonal (45°E - 75°E) 10-day (12-21 June 1979) means of (a) southerly wind component (v) in m $s^{-1}$ and (b) westerly wind component in m $s^{-1}$; (c) and (d) are Kuo simulations of (a) and (b); (e) and (f) are A-S simulations of (a) and (b).

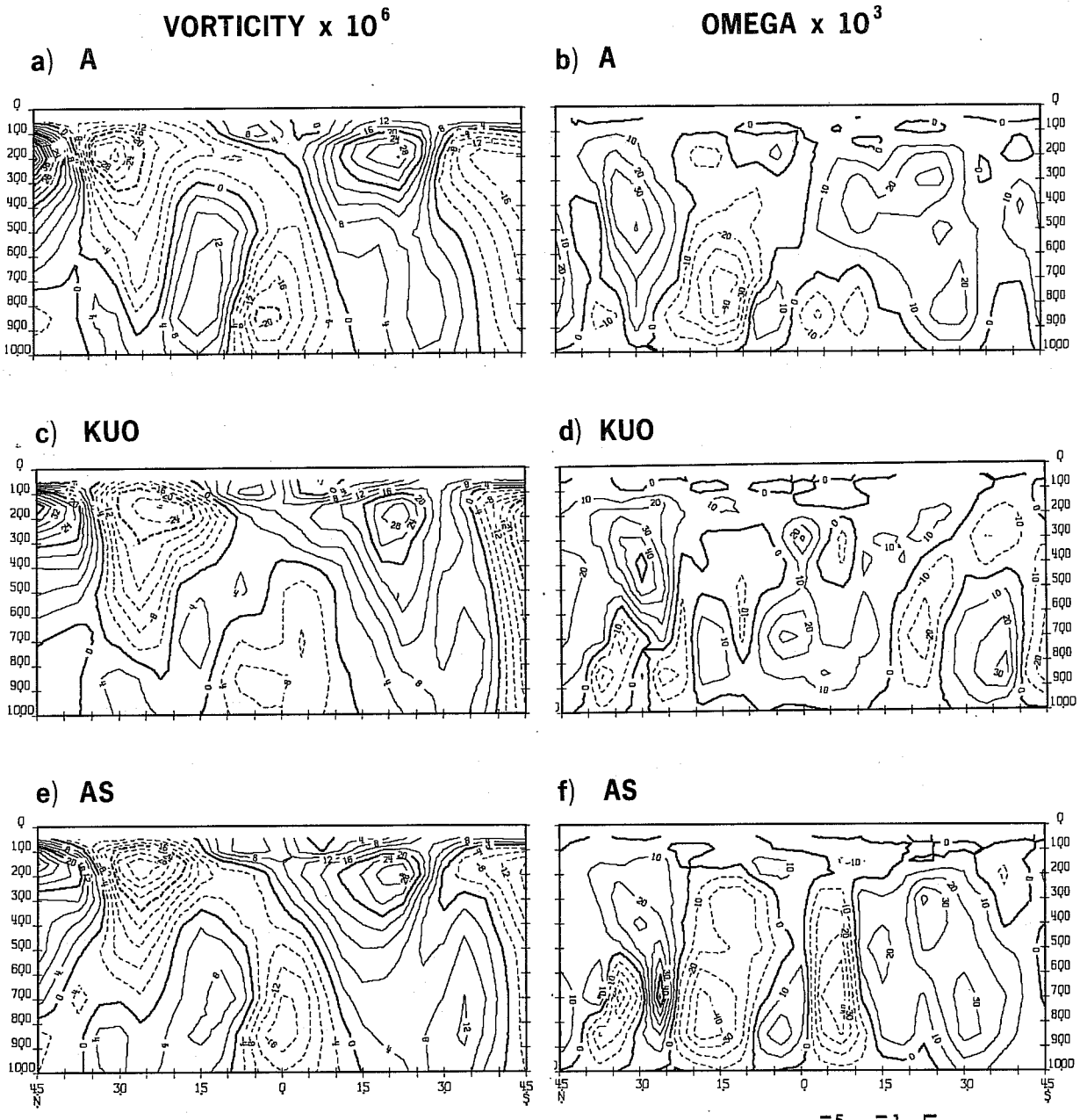


Fig. 22 As Fig. 20 but for relative vorticity ($\zeta$) in $10^{-5}$ $s^{-1}$ [(a), (c), (e)] and vertical motion ($\omega$) in $10^{-3}$ Pa $s^{-1}$ [(b), (d), (f)].

are mainly due to the fact that the onset of the monsoon in the model is delayed by about 10 day (Fig. 2(c)). Further, the A-S simulations are closer than the Kuo simulations to the FGGE analyses in most respects:

(i) The low level westerlies and upper level easterlies over the Arabian Sea are better simulated (Fig. 21) with consequent better simulation of the vorticity in this region (Fig. 22);

(ii) The ascent over the Arabian Sea is well simulated both in strength and position, with the maximum value at about 800 mb (Fig. 22(f)). There is, however, a second maximum near 8°S, extending throughout the troposphere, not present in the FGGE analyses (Fig. 22b);

However over the 75°E - 105°E region (cross-sections not reproduced here) the A-S ascent is even stronger and less like that from the FGGE analyses than the Kuo simulation, with an additional maximum in the Southern Hemisphere.

## 5. SUMMARY OF MAIN RESULTS AND DISCUSSION

The main features of the low-level monsoonal flow over the Arabian Sea, i.e. the Somali jet and westerlies, were present in the initial data (11 June, 12Z); also at this stage the upper easterlies were present over a substantial part of the tropical Indian Ocean, although only at about half of their strength during the fully established monsoon. Nevertheless, the model did not immediately produce the observed intensification of the low-level flow over the Arabian Sea with either the Kuo or Arakawa-Schubert convection scheme.

Other aspects of the observed development not adequately simulated by the model integrations were:

(i) the band of upper north-easterlies across the equator extending over virtually the whole of the Indian Ocean, merging with the Southern Hemisphere sub-tropical jet;

(ii) the low-level northerlies across Saudi Arabia;

(iii) the full depth and strength of the low-level monsoon westerlies (Kuo Scheme);

(iv) the correct mean moisture and temperature over the Arabian Sea region.

The deficiencies identified by these experiments must be attributed to all or any of three primary sources:

(i) errors in the initial analyses

(ii) errors arising from the model initialisation procedure, and

(iii) model deficiencies, particularly the convective parameterisation scheme.

The quality of the initial analyses is dictated by the quality and coverage of the FGGE data. However, although errors in the initial analyses are important for the model flow development in the early stages, they are presumably less significant in general for the mean flow patterns for a 10-day period as presented here. An exception could be over North Africa where the 850 mb winds are particularly unrealistic in both simulations, possibly contributing to the failure of the low-level winds to intensify over the Arabian Sea.

It is well recognised that the non-linear normal mode initialisation scheme used in these experiments is not very suitable for the tropics as it reduces the divergent component of the wind by a factor of at least 2 (Bengtsson, 1980). With such underestimates, particularly in the regions of low-level convergence, the Kuo scheme cannot operate as effectively as it should and the moisture-controlled convective 'spin-up' will be too slow initially. On the other hand, the A-S scheme, basically a generalised adjustment scheme, is unlikely to be as much affected.

The model initial moisture distributions are obtained using vertical interpolation (from p- to $\sigma$-surfaces) of incremental differences between observations and first guess fields; those used for the FGGE analyses were based on interpolations of the full values. This is the explanation of the differences between the Arabian Sea mean moisture values used as initial data for the integrations and the FGGE analyses for June 11th in Figs. 2(a) and 14(a).

In view of these differences it is possible to discuss the behaviour of the two convection schemes over the Arabian Sea only by comparing the simulated trends in moisture and temperature with the FGGE analyses. A marked drying out and cooling occurs during the first ten days with both schemes. The drying-out is more pronounced for the A-S scheme indicating that it produces more convective rain over the region than the Kuo scheme. This is consistent with the A-S mean temperatures (Fig. 14(b)) falling much less rapidly than those for the Kuo scheme. Interestingly, the A-S moisture values (Fig. 14(a)) agree well with the FGGE values after two days, whereas the Kuo scheme values remain relatively high for ten days.

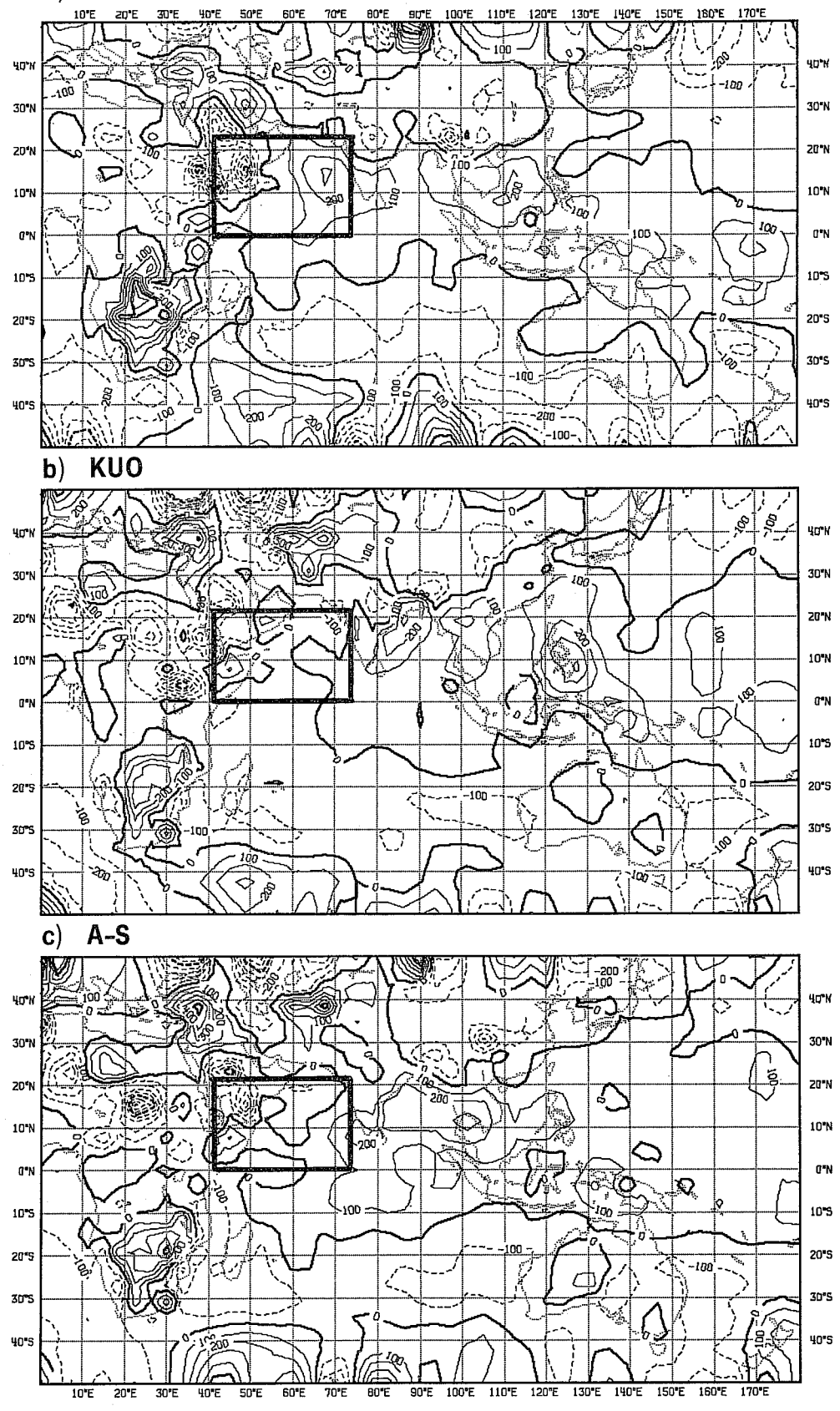


Fig. 23 Mean net tropospheric heating (W m$^{-2}$) from 1200Z on 12 June to 1200Z on 21 June, 1979 (a) from FGGE analyses, (b) from Kuo simulation and (c) from A-S simulation. The Arabian Sea area is outlined.

In order to extend the comparisons to a larger area the ten-day average tropospheric heating ($\bar{Q}$) is shown in Figs. 23(a) to (c) for hemispheric tropical strip between 45°S and 45°N. $\bar{Q}$ may be written as

$$\bar{Q} = \bar{Q}_L + \bar{Q}_{SC} + \bar{Q}_{Rad}$$

where the suffices relate respectively to latent heat release, sensible heating by convection and radiative heating. Then since $\bar{Q}_{Rad}$ is typically -100 to -200 W $m^{-2}$ and $\bar{Q}_{SC}$ is small over the ocean, it can be assumed that latent heat release has occurred for all oceanic regions where $\bar{Q}$ is greater than -100 W $m^{-2}$. Most of this is associated with convective rainfall, i.e. needs to be produced in the model by the convection scheme, 100 W $m^{-2}$ corresponding to about 4 mm of rain per day. Fig. 23 shows a maximum of 300 W $m^{-2}$ heating in the eastern Arabian Sea, not reproduced by either of the model simulations. The A-S scheme produces a maximum of 200 W $m^{-2}$ just off Sri Lanka but the Kuo scheme maximum of 300 W $m^{-2}$ is well to the east over the Bay of Bengal. The heating patterns show that both schemes generate regions of high mean convective rainfall but not where it actually occurs; too little is produced in the Arabian Sea and too much in the Bay of Bengal.

It is possible, therefore, that during the first two days or so, while the model convection scheme is adjusting to the larger-scale dynamics, regions of low-level mass (and moisture) convergence develop in regions dictated largely by the requirements of the particular convection scheme adopted and the initial data (particularly the humidity field). Any errors introduced during this period have a major influence on subsequent model developments. In the case described here too little convection became established in the first two days over the Arabian Sea and too much over the Bay of Bengal, setting up a large-scale rainfall pattern different from the observed which persisted for the next eight days or so.

These results clearly demonstrate the sensitivity of the model simulation of the monsoon onset to the convective parameterisation. This is presumably a consequence of the monsoon being a form of large-scale convective organisation, involving both hemispheres, in which moist lower boundary-layer air is rapidly transported in deep moist convective systems over the Indian sub-continent and adjacent oceans to the upper troposphere; here it forms an outflow extending across the equator well into the Southern Hemisphere. Its intensification is dictated by release of convective instability and accurate simulation of the rapid intensification phase of the onset must thus be expected to require the model's convection scheme to be a very realistic one. It could well be that, for instance, such a scheme must include parameterisation of cumulus-scale momentum transfer. Further there is a need to improve the analyses of specific humidity over the tropics - the slow spin up of model's convection could result from errors in the humidity analysis.

The problems highlighted by this study are already generally recognised as presenting a major challenge to numerical modellers. The FGGE data set provides the best opportunity to date to resolve them and simulation of the monsoon onset probably one of the most sensitive tests.

Acknowledgements

The authors are most grateful to Dr.D. Burridge, Dr.A. Hollingsworth, Dr.R. Riddaway and Dr.W. Heckley for their helpful discussions and suggestions which led to improvements in the manuscript. We also thank Mrs.N. Spicer who typed many sections of the original manuscript.

REFERENCES


Arakawa, A. and W.H. Schubert, 1974: Interaction of a cumulus cloud ensemble with the large-scale environment. Part I: J.Atmos.Sci., 31, 674-701.

Bengtsson, L., 1981 Current problems in four-dimensional data assimilation. Seminar on Data Assimilation Methods, ECMWF, 195-218.

Bengtsson, L., M. Kanamitsu, P.Kallberg, and S. Uppala, 1982: FGGE 4-dimensional data assimilation at ECMWF. Bull.Amer.Met.Soc., 63, 29-43.

Burridge, D.M. and J. Haseler, 1977: A model for medium range weather forecasting - adiabatic formulation. ECMWF Tech.Rep.No.4.

Kuo, H.L., 1965: On formation and intensification of tropical cyclones through latent heat release by cumulus convection. J.Atmos.Sci., 22, 40-63.

Kuo, H.L., 1974 Further studies of the parameterization of the influence of cumulus convection on large-scale flow. J.Atmos.Sci., 31, 1232-1240.

Lönnberg, P. and D. Shaw, 1983: ECMWF data assimilation scientific documentation. ECMWF Meteorological bulletin M1.5/1. Research manual 1.

Lord, S.J., 1982: Interaction of a cumulus cloud ensemble with the large-scale environment. Part III: Semi-prognostic test of the Arakawa-Schubert cumulus parameterization. J.Atmos.Sci., 39, 88-103.

Lord, S.J., W.C.Chao, and A. Arakawa, 1982: Interaction of a cumulus cloud ensemble with the large-scale environment. Part IV: The discrete model. J.Atmos.Sci., 39, 104-113.

Lorenc, A.C., 1981: A global three-dimensional multivariate statistical interpolation scheme. Mon.Wea.Rev., 109, 701-721.

O'Brien, J.J., 1970: Alternative solutions to the classical vertical velocity problem. J.Appl.Meteor., 9, 197-203.

Pearce, R.P. and Mohanty, U.C., 1984 Onsets of the Asian summer monsoon 1979-82. J.Atmos.Sci., 41, 1620-1639.

Simmons, A.J., 1982: The numerical prediction and simulation of the tropical atmosphere - a sample of results from operational forecasting and extended integrations at ECMWF. Tropical droughts: Meteorological aspects and implications for agriculture. R.P.Pearce (ed). WMO, Geneva, 81-103.

Tiedtke, M., J.-F.Geleyn, A. Hollingsworth and J.-F. Louis, 1979: ECMWF model parameterization of sub-grid scale processes. ECMWF Tech.Rep.No.10, 46pp.

Tiedtke, M., 1984: The effect of penetrative cumulus convection on the large-scale flow in a general circulation model. Contrib.Atmos Phys., 57,216-239.

Tiedtke, M., 1985: Description of the ECMWF version of the Arakawa-Schubert convection scheme. ECMWF Tech.Rep. (to be published).

ECMWF PUBLISHED TECHNICAL REPORTS

No.1 A Case Study of a Ten Day Prediction

No.2 The Effect of Arithmetic Precisions on some Meteorological Integrations

No.3 Mixed-Radix Fast Fourier Transforms without Reordering

No.4 A Model for Medium-Range Weather Forecasting - Adiabatic Formulation

No.5 A Study of some Parameterizations of Sub-Grid Processes in a Baroclinic Wave in a Two-Dimensional Model

No.6 The ECMWF Analysis and Data Assimilation Scheme - Analysis of Mass and Wind Fields

No.7 A Ten Day High Resolution Non-Adiabatic Spectral Integration: A Comparative Study

No.8 On the Asymptotic Behaviour of Simple Stochastic-Dynamic Systems

No.9 On Balance Requirements as Initial Conditions

No.10 ECMWF Model - Parameterization of Sub-Grid Processes

No.11 Normal Mode Initialization for a Multi-Level Gridpoint Model

No.12 Data Assimilation Experiments

No.13 Comparisons of Medium Range Forecasts made with two Parameterization Schemes

No.14 On Initial Conditions for Non-Hydrostatic Models

No.15 Adiabatic Formulation and Organization of ECMWF's Spectral Model

No.16 Model Studies of a Developing Boundary Layer over the Ocean

No.17 The Response of a Global Barotropic Model to Forcing by Large-Scale Orography

No.18 Confidence Limits for Verification and Energetic Studies

No.19 A Low Order Barotropic Model on the Sphere with the Orographic and Newtonian Forcing

No.20 A Review of the Normal Mode Initialization Method

No.21 The Adjoint Equation Technique Applied to Meteorological Problems

No.22 The Use of Empirical Methods for Mesoscale Pressure Forecasts

No.23 Comparison of Medium Range Forecasts made with Models using Spectral or Finite Difference Techniques in the Horizontal

No.24 On the Average Errors of an Ensemble of Forecasts

ECMWF PUBLISHED TECHNICAL REPORTS

No.25 On the Atmospheric Factors Affecting the Levantine Sea

No.26 Tropical Influences on Stationary Wave Motion in Middle and High Latitudes

No.27 The Energy Budgets in North America, North Atlantic and Europe Based on ECMWF Analyses and Forecasts

No.28 An Energy and Angular-Momentum Conserving Vertical Finite-Difference Scheme, Hybrid Coordinates, and Medium-Range Weather Prediction

No.29 Orographic Influences on Mediterranean Lee Cyclogenesis and European Blocking in a Global Numerical Model

No.30 Review and Re-assessment of ECNET - a Private Network with Open Architecture

No.31 An Investigation of the Impact at Middle and High Latitudes of Tropical Forecast Errors

No.32 Short and Medium Range Forecast Differences between a Spectral and Grid Point Model. An Extensive Quasi-Operational Comparison

No.33 Numerical Simulations of a Case of Blocking: the Effects of Orography and Land-Sea Contrast

No.34 The Impact of Cloud Track Wind Data on Global Analyses and Medium Range Forecasts

No.35 Energy Budget Calculations at ECMWF: Part I: Analyses

No.36 Operational Verification of ECMWF Forecast Fields and Results for 1980-1981

No.37 High Resolution Experiments with the ECMWF Model: a Case Study

No.38 The Response of the ECMWF Global Model to the El-Nino Anomaly in Extended Range Prediction Experiments

No.39 On the Parameterization of Vertical Diffusion in Large-Scale Atmospheric Models

No.40 Spectral characteristics of the ECMWF Objective Analysis System

No.41 Systematic Errors in the Baroclinic Waves of the ECMWF Model

No.42 On Long Stationary and Transient Atmospheric Waves

No.43 A New Convective Adjustment Scheme

No.44 Numerical Experiments on the Simulation of the 1979 Asian Summer Monsoon